HE 1158

PERGAMON

International Journal of Hydrogen Energy 000 (2000) 000–000

International Journal of HYDROGEN ENERGY

www.elsevier.com/locate/ijhydene

Synthesis and characterization of novel hydride compounds

Randell L. Mills *, Bala Dhandapani, Mark Nansteel, Jiliang He, Tina Shannon, Alex Echezuria

BlackLight Power, Inc., 493 Old Trenton Road, Cranbury, NJ 08512, USA

Abstract

Novel inorganic alkali and alkaline earth hydrides of the formula MHX and MHMX wherein M is the metal, X, is a singly negatively charged anion, and H comprises a novel high binding energy hydride ion were synthesized in a high temperature gas cell by reaction of atomic hydrogen with a catalyst and MX or MX_2 corresponding to an alkali metal or alkaline earth metal compound, respectively. Novel hydride compounds were identified by time of flight secondary ion mass spectroscopy, X-ray photoelectron spectroscopy, proton nuclear magnetic resonance spectroscopy, and thermal decomposition with analysis by gas chromatography, and mass spectroscopy.

1. Introduction

Typically the emission of extreme ultraviolet light from hydrogen gas is achieved via a discharge at high voltage, a high power inductively coupled plasma, or a plasma created and heated to extreme temperatures by RF coupling (e.g. $> 10^6$ K) with confinement provided by a toroidal magnetic field. Intense extreme ultraviolet (EUV) emission was observed at low temperatures (e.g. $\approx 10^3$ K) from atomic hydrogen and certain atomized elements or certain gaseous ions which ionize at integer multiples of the potential energy of atomic hydrogen [1–6]. For example, strontium ionizes at integer multiples of the potential energy of atomic hydrogen. Intense EUV hydrogen plasma emission was observed at low temperatures (e.g. $\approx 10^3$ K) when atomic hydrogen was generated at a tungsten filament that heated a titanium dissociator and atomic strontium was vaporized from the metal by heating. No emission was observed when sodium, magnesium, or barium replaced strontium or when argon replaced hydrogen with strontium. Furthermore, the power balance of a gas cell having atomized hydrogen and strontium was measured by integrating the total light output corrected for detector response and energy over the visible range [6]. A control cell was identical except that sodium replaced strontium. In this case, over 4000 times the power of the strontium cell was required in order to achieve that same optically measured light output power. A plasma formed at a cell voltage of about 250 V in the cell with hydrogen alone and in the cell with hydrogen and sodium; whereas, a plasma formed in the strontium cell at the extremely low voltage of about 2 V.

Based on their exceptional emission, we used potassium, cesium, rubidium, calcium, and strontium metals as catalysts to release energy from atomic hydrogen to form novel compounds [1,2]. The theory is given in the Appendix.

Novel inorganic alkali and alkaline earth hydrides of the formula MHX and MHMX wherein M is the metal, X, is a singly negatively charged anion, and H comprises a novel high binding energy hydride ion were synthesized in a high-temperature gas cell by reaction of atomic hydrogen with a catalyst and MX or MX_2 corresponding to an alkali metal or alkaline earth metal compound, respectively. For example, atomic hydrogen was reacted with strontium vapor and $SrBr_2$ to form SrHBr. Novel hydride compounds such as SrHBr were identified by time of flight secondary ion mass spectroscopy, X-ray photoelectron spectroscopy, proton nuclear magnetic resonance spectroscopy, and thermal decomposition with analysis by gas chromatography,

* Corresponding author. Tel.: +1-609-490-1040; fax: +1-609-490-1066.

E-mail address: rmills@blacklightpower.com (R.L. Mills).

0360-3199/00/$ 20.00
PII: S0360-3199(00)00113-0

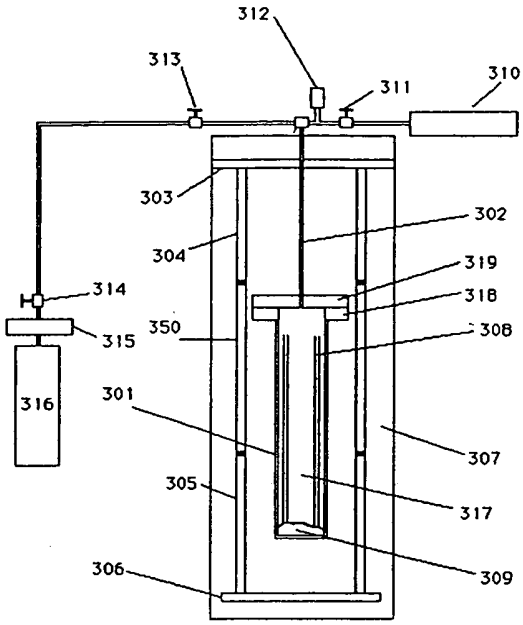

Fig. 1. Stainless steel gas cell comprising a screen dissociator, metal catalyst, and alkali or alkaline earth halide as the reactant. The components were: 301 — stainless steel cell; 317 — internal cavity of cell; 318 — high vacuum conflat flange; 319 — mating blank conflat flange; 302 — stainless steel tube vacuum line and gas supply line; 303 — lid to the kiln or top insulation, 304, 305, 350, and 306 — heaters; 307 — high temperature insulation; 308 — screen dissociator; 309 — powdered alkali or alkaline earth halide reactant; 310 — high vacuum turbo pump; 312 — pressure gauge; 311 — vacuum pump valve; 313 — valve; 314 — valve; 315 — regulator; 316 — hydrogen tank.

and mass spectroscopy. Hydride ions with increased binding energies form novel compounds with potential broad applications such as a high-voltage battery for consumer electronics and electric vehicles. In addition, these novel compositions of matter and associated technologies may have far-reaching applications in many industries including chemical, electronics, computer, military, energy, and aerospace in the form of products such as propellants, solid fuels, surface coatings, structural materials, and chemical processes.

2. Experimental

2.1. Synthesis

2.1.1. Potassium iodo hydride, KHI, synthesis in a 3.0 l stainless steel reactor

Potassium iodo hydride was prepared in a stainless steel gas cell shown in Fig. 1 comprising a Ni screen hydrogen dissociator (Belleville Wire Cloth Co., Inc.), potassium metal catalyst (Aldrich Chemical Company), and KI (Aldrich Chemical Company 99.9%). The 316-stainless steel cell was in the form of a tube having an internal cavity of 375 mm in length and 140 mm in diameter. The wall thickness was 6.35 mm. The bottom of the cell was closed by a 6.35 mm thick circular plate of 316 stainless steel that was welded to the cylinder. The top end of the cell was welded to a bored-through 304 stainless steel conflat-type flange with 8 in nominal diameter. A mating blank flange was bolted to the bored-through flange with 20 silver-plated bolts. A flange gasket was silver-plated copper. A 1.27 cm OD tube was welded into a hole at the center of the blank flange. This tube was closed at one end and extended 20 cm into the reactor, serving as a thermowell. A 9.5 mm OD stainless tube was welded to the flange approximately 4 cm from the flange center. This tube served as the vacuum line from the cell as well as a hydrogen or helium supply line to the cell.

The reactor was heated in a 10 kW refractory brick kiln (L & L Kiln Model JD230). The kiln had three heating zones and a heated floor that were each heated by separate radiant elements. The zone temperatures were independently controlled by a Dynatrol controller. The reactor was instrumented with 5 type-K thermocouples. Two thermocouples were located in the central thermowell at approximately reactor mid-height and at flange- level. Three thermocouples were fixed to the external surface of the reactor and were located near the base, at mid-height, and near flange- level. The reactor was connected through bellows-type valves to a turbo vacuum pump. The vacuum level was measured by a 0–100 Torr Baratron vacuum gauge. Pressures above 100 Torr were measured by standard dial-type pressure gauges. Temperature and pressure data was logged to a data acquisition system at 5 min intervals.

Approximately 290 g of nickel screen (0.5 mm wire, 2 mm mesh) was placed circumferentially around the reactor inner wall of the cell. 125 g of dry KI were placed in a stainless steel crucible on the reactor base. The reactor was flooded with argon gas. 1.7 g of metallic potassium was placed in a smaller stainless steel crucible and this crucible was placed in the larger one with the KI crystals. The reactor was sealed and placed in the kiln. The system was evacuated for 2.5 h. The reactor was pressurized with hydrogen gas to a pressure of 10 Torr and sealed. The kiln was heated to 650°C at the rate of 300°C/h. The reactor was held at 650°C for 72 h. Hydrogen was added to the system periodically to maintain a pressure level of 10 Torr. The reactor was then evacuated for 1 h while at 650°C. The kiln and reactor were cooled to room temperature by forced convection in about 2 h while pumping continued. At room temperature the system was filled with helium gas to a pressure of 1.3 bar. The sealed reactor was then opened. About 125 g of green crystals were observed to have formed in the stainless steel crucible.

2.1.2. Strontium fluoro hydride synthesis in a 40 cm^3 stainless steel gas cell reactor

Strontium fluoro hydride was prepared in a stainless steel gas cell shown in Fig. 1 comprising a Ti screen hydrogen

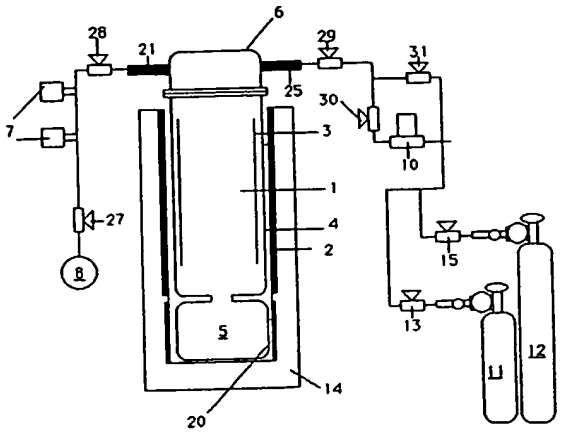

Fig. 2. Quartz gas cell comprising a Ni screen dissociator, potassium metal catalyst, and K_2CO_3 as the reactant. The components were: 1 — internal cavity of cell; 3 — nickel hydrogen dissociator; 4 — quartz tube cell with Conflat style flange; 5 — catalyst reservoir; 6 — Pyrex cap with an identical Conflat style flange to the tube; 25 — gas inlet line; 21 — gas outlet line; 11 — compressed gas cylinder of ultra high purity hydrogen; 13 — hydrogen control valve; 12 — compressed gas cylinder of ultrahigh purity helium; 15 — helium control valve; 10 — mass flow controller; 30 — mass flow controller valve; 29 — inlet valve; 31 — mass flow controller bypass valve; 8 — molecular drag pump; 27 — vacuum pump valve; 28 — outlet valve; 7 — 0 to 1000 torr Baratron pressure gauge and a 0 to 100 torr Baratron pressure gauge; 20 — catalyst reservoir band heater; 14 — Zircar AL-30 insulation package; 2 — Mellen cell heater.

dissociator (Belleville Wire Cloth Co., Inc.), strontium metal catalyst (Alfa Aesar), and SrF_2 (Aldrich Chemical Company, 99.99%) as the reactant. The 304-stainless steel cell was in the form of a tube having an internal cavity of 75 mm in length and 28 mm in diameter. The top end of the cell was welded to a high vacuum 2 $\frac{3}{4}$ in bored through conflat flange. The mating blank conflat flange contained a single opening in which was welded a $\frac{1}{4}$ in diameter stainless steel tube that was 10 cm in length and contained a needle valve to isolate the reactor from the rest of the gas manifold. A silver plated copper gasket was placed between the two flanges. The two flanges are held together with 6 circumferential bolts. The bottom of the $\frac{1}{4}$ in tube was flush with the bottom surface of the top flange. The $\frac{1}{4}$ in tube served as a vacuum line and also as a hydrogen or helium supply line to the cell. The cell was surrounded by a clam shell heater (Mellen Company), which was in turn surrounded by insulation. The heater was controlled by a Variac.

About 10 g of Ti screen, 12 g of crystalline SrF_2 and 0.6 g of strontium metal was added to the cell under an argon atmosphere. The cell was then continuously evacuated with the isolation needle valve open using a high vacuum turbo pump to reach 20 mTorr measured by a pressure gauge (MKS). The cell was heated by supplying power to the heaters. The temperature of the cell was measured with a type K thermocouple (Omega). The cell temperature was then slowly increased to 100°C using the heaters. The vacuum pump valve was closed. Hydrogen was slowly added to maintain a pressure of 1 atm, and the needle valve was closed to isolate the reactor system. The temperature of the cell was then slowly increased to 650°C. Hydrogen was added periodically to maintain 1 atm using the needle valve. After 72 h, the temperature of the cell was reduced to room temperature. The reactor was flushed with helium and closed using the needle valve. It was then opened in an argon environment chamber to recover the strontium fluoro hydride. A white solid was obtained.

2.1.3. Potassium hydride potassium hydrogen carbonate synthesis in a quartz gas cell reactor

Potassium hydride potassium hydrogen carbonate was prepared in a quartz gas cell shown in Fig. 2 comprising a nickel screen hydrogen dissociator (Belleville Wire Cloth Co., Inc.), potassium metal catalyst (Aldrich Chemical Company), and K_2CO_3 (Aldrich Chemical Company 99.9%) as the reactant. The quartz cell was in the form of a tube having an internal cavity of fifty (50) millimeters in diameter and five hundred (500) millimeters in length. One end of the cell was necked down and attached to a fifty (50) cubic centimeter catalyst reservoir. The other end of the cell was fitted with a Conflat style high vacuum flange that was mated to a Pyrex cap with an identical Conflat style flange. A high vacuum seal was maintained with a Viton O-ring and stainless steel clamp. The Pyrex cap included two glass-to-metal tubes for the attachment of a gas inlet line and gas outlet line.

H_2 gas was supplied to the cell through the inlet from a compressed gas cylinder of ultra high-purity hydrogen controlled by a hydrogen control valve. Helium gas was supplied to the cell through the same inlet from a compressed gas cylinder of ultrahigh purity helium controlled by helium control valve. The flow of helium and hydrogen to the cell is further controlled by a mass flow controller, a mass flow controller valve, an inlet valve, and a mass flow controller bypass valve. The bypass valve was closed during filling of the cell. Excess gas was removed through the gas outlet by a molecular drag pump capable of reaching pressures of 10^{-4} Torr controlled by vacuum pump valve and outlet valve. Pressures were measured by a 0–10 Torr Baratron pressure gauge. The reactor and the catalyst reservoir, were heated independently using clam shell heaters (Mellen Company) powered by Variacs. The temperature was recorded using a K-type thermocouple placed close to the quartz reactor.

The cell was operated under flow conditions with a total pressure of less than two (2) Torr of hydrogen or control helium via mass flow controller. About 20 g of K_2CO_3 (Aldrich Chemical Company, 99.9%) was placed in the

catalyst reservoir and about 50 g, 12 × 12 cm of nickel screen dissociator (Belleville Wire Cloth Co., Inc.) was treated with 0.6 M K_2CO_3/10% H_2O_2 and dried at 130°C overnight and then placed in the center of the reactor. The reactor was evacuated to about 50 mTorr and hydrogen was introduced using the mass flow controller to maintain a pressure of about 2 Torr. The temperature of the reactor was increased to about 800–850°C to facilitate atomization of hydrogen, and the catalyst reservoir temperature was increased to 850°C to vaporize the catalyst. The reaction started when the catalyst vapor reached the hot zone of the reactor. The reaction was allowed to continue for about 120 h. The reaction was terminated by cooling the reactor and the catalyst reservoir to room temperature in hydrogen. The system was purged and back filled with helium and sealed. The reactor was opened in an argon environmental chamber and the samples were collected and analyzed. The compound was a white powder.

2.1.4. Synthesis of alkali halido hydrides and alkaline earth halido hydrides

A series of alkali and alkaline earth halido hydrides (KHF, KHCl, KHBr, KHI, RbHF, RbHCl, RbHBr, RbHI, CsHF, CsHCl, CsHBr, CsHI, CaHCl, CaHBr, CaHI, SrHF, SrHCl, and SrHBr) were synthesized in gas cells as described in the previous A–B Sections with the exception that the alkali or alkaline earth metal catalyst (rubidium metal (which is a catalyst as a hydride having Rb^+) and potassium, cesium, calcium, and strontium metals) corresponded to the alkali or alkaline earth halide of the product alkali or alkaline earth halido hydride. RbHF was synthesized by the catalysis of atomic hydrogen with potassium metal catalyst followed by reaction with RbF wherein the hydrogen dissociator was a nickel screen. Reactants to form hydrides of these inorganic compounds obtained from Alfa Aesar were KF (99.9%), KCl (ACS grade 99+(99.9%)), RbI (99.9%), CsF (99.9%), CsCl (99.9%), CsBr (99.9%), CsI (99.9%), $CaCl_2$ (99.9%), $CaBr_2$ (99.9%), CaI_2 (99.9%), SrF_2 (99.9%), $SrCl_2$ (99.9%), and $SrBr_2$ (99.9%). In the analytical analyses, each starting compound was also used as a control.

2.2. ToF–SIMS characterization

The crystalline samples were sprinkled onto the surface of a double-sided adhesive tape and characterized using a Physical Electronics TFS-2000 ToF-SIMS instrument. The primary ion gun utilized a $^{69}Ga^+$ liquid metal source. In order to remove surface contaminants and expose a fresh surface, the samples were sputter cleaned for 30 s using a 40 μm × 40 μm raster. The aperture setting was 3, and the ion current was 600 pA resulting in a total ion dose of 10^{12} ions/cm^2.

During acquisition, the ion gun was operated using a bunched (pulse width 4 ns bunched to 1 ns) 15 kV beam [7,8].[1] The total ion dose was 10^{12}ions/cm^2. Charge neutralization was active, and the post accelerating voltage was 8000 V. Three different regions on each sample of $(12\ \mu m)^2$, $(18\ \mu m)^2$, and $(25\ \mu m)^2$ were analyzed. The positive and negative SIMS spectra were acquired. Representative post sputtering data is reported.

2.3. XPS characterization

A series of XPS analyses were made on the crystalline samples of KHCl and KCl using a Scienta 300 XPS Spectrometer. The fixed analyzer transmission mode and the sweep acquisition mode were used. The step energy in the survey scan was 0.5 eV, and the step energy in the high resolution scan was 0.15 eV. In the survey scan, the time per step was 0.4 s, and the number of sweeps was 4. In the high resolution scan, the time per step was 0.3 s, and the number of sweeps was 30. C 1s at 284.5 eV was used as the internal standard.

The binding energies and features of core level electrons of a series of alkali and alkaline earth halido hydrides (KHCl, KHI, RbHCl, RbHI, CsHBr, CaHCl, CaHBr, CaHI, SrHF, SrHCl, and SrHBr) were analyzed by XPS. XPS analysis was conducted on a Kratos XSAM-800 spectrometer using nonmonochromatic Al Kα (1468.6 eV) radiation. Samples were crushed in a glove box under argon and mounted on an analysis stub with copper tape. A piece of gold foil was stuck into the sample for calibration. The samples were transferred under an inert atmosphere. A survey spectrum was run from 1000 to 0 eV. For quantitative analysis, high resolution spectra were run on core level electrons of interest such as the Rb3d and Cs3d electrons. For KI and KHI, a high resolution spectrum of the low binding energy region was also run from 100 to 0 eV that corresponded to the survey spectrum. Fixed analyzer transmission (FAT) mode was used in all measurements. For the survey scan, a pass energy of 320 eV was employed. A pass energy of 40 eV was used for high resolution scans. In the cases were a charging effect was observed, the spectrum was corrected by using a calibration of the effect with the $Au4f_{7/2}$ peak at 84.0 eV as a first standard and the C1s peak at 284.6 eV as a second standard.

2.4. NMR spectroscopy

^{1}H MAS NMR was performed on solid samples of KHI, KHCl, KHBr, and RbHF. The data was obtained on a custom built spectrometer operating with a Nicolet 1280 computer. Final pulse generation was from a tuned Henry radio amplifier. The ^{1}H NMR frequency was 270.6196 MHz. A 5 μ s pulse corresponding to a 41° pulse length and a 3 recycle delay were used. The window was ±20 kHz. The spin speed was 4.0 kHz. (The spin speed was varied to confirm real peaks versus side bands. The latter changed

[1] For recent specifications see Ref. [8].

position with spin speed, the former were independent of spin speed.) The number of scans was 600. The offset was 1541.6 Hz, and the magnetic flux was 6.357 T. The samples were handled under a nitrogen atmosphere. Chemical shifts were referenced to external tetramethylsilane (TMS). The reference of KHI comprised KH (Aldrich Chemical Company 99%) and equivalent molar mixtures of KH (Aldrich Chemical Company 99%) and KI (Aldrich Chemical Company 99.99%) prepared in a glove box under argon. The reference of KHCl comprised KH (Aldrich Chemical Company 99%) and equivalent molar mixtures of KH (Aldrich Chemical Company 99%) and KCl (Aldrich Chemical Company 99.99%) prepared in a glove box under argon. The reference of KHBr comprised KH (Aldrich Chemical Company 99%) and equivalent molar mixtures of KH (Aldrich Chemical Company 99%) and KBr (Aldrich Chemical Company 99.99%) prepared in a glove box under argon. The reference of RbHF comprised RbH (Aldrich Chemical Company 99%).

^{1}H MAS NMR was performed on a solid samples of SrHBr. The data were recorded on a Bruker DSX-300 spectrometer at 300.132 MHz. Samples were packed and sealed in 5 mm diameter NMR tubes under an inert atmosphere. The ^{1}H MAS NMR of strontium bromo hydride was run static. The MAS frequency was 4.1 kHz. During data acquisition, the 90° pulse length for a single pulse ^{1}H excitation was 3.4 μs; the sweep width was 147.058 kHz; the dwell time was 5.5 μs, and the acquisition time was 0.0139764 s/scan. The number of scans was typically 32.

The hydrogen composition of the samples was quantified by integrating the signal under each peak. In each case, the signal from an empty tube was baseline subtracted from the integral for each peak. The integration was calibrated using a polyethylene standard. From the sample weight, the wt% hydrogen was determined. The chemical shifts of the spectra were calibrated based on the chemical shift of H_2O. The accuracy was determined to be within 0.1 ppm. Some samples were broadened due to ^{1}H–^{1}H dipole interactions. The broadening from a neighboring proton interaction was 120 kHz/r^3. Given the NMR frequency of 300 MHz, there were 300 Hz per ppm. As an example, peak widths of 7 ppm correspond to 2.1 kHz. Based on this frequency, the distance to a neighboring proton is ~4 Å. Motion of the protons could result in line narrowing.

2.5. Thermal decomposition with analysis by gas Chromatography

Solid samples were decomposed at high temperature and quantitatively analyzed for hydrogen using gas chromatography. 0.1 g of sample was placed in a thermal decomposition reactor under an argon atmosphere. The reactor comprised a 1/4" OD by 3" long quartz tube that was sealed at one end and connected at the open end with Swagelock™ fittings to a T. One end of the T was connected to a needle valve and a HOVAC molecular drag pump. The other end was attached to a septum port. The apparatus was evacuated to between 25 and 50 m Torr. The needle valve was closed to form a gas tight reactor. The sample was heated in the evacuated quartz chamber containing the sample with an external Nichrome wire heater using a Variac transformer. The sample was heated to above 600°C by varying the transformer voltage supplied to the Nichrome heater until the sample melted. Gas released from the sample was collected with a 500 μl gas tight syringe through the septum port and immediately injected into the gas chromatograph.

Gas samples were analyzed with a Hewlett Packard 5890 Series II gas chromatograph equipped with a thermal conductivity detector and a 60 m, 0.32 mm ID fused silica Rt-Alumina capillary PLOT column (Restek, Bellefonte, PA). The column was conditioned at 200°C for 18–72 h before each series of runs. Samples were run at −196°C using Ne as the carrier gas. The 60 m column was run with the carrier gas at 3.4 psi with the following flow rates: carrier — 2.0 ml/min, auxiliary — 3.4 ml/min and reference — 3.5 ml/min, for a total flow rate of 8.9 ml/min. The split rate was 10.0 ml/min.

The control hydrogen gas was ultrahigh purity (MG Industries). Control samples were also treated by the same method as the samples of the novel compounds.

2.6. Thermal decomposition with analysis by mass spectroscopy

Mass spectroscopy was performed on the gases released from the thermal decomposition of the samples. One end of a 4 mm ID fritted capillary tube containing about 5 mg of sample was sealed with a 0.25 in. Swagelock union and plug (Swagelock Co., Solon, OH). The other end was connected directly to the sampling port of a Dycor System 1000 Quadrapole Mass Spectrometer (Model D200MP, Ametek, Inc., Pittsburgh, PA with a HOVAC Dri-2 Turbo 60 Vacuum System). The capillary was heated with a Nichrome wire heater wrapped around the capillary. The mass spectrum was obtained at the ionization energy of 70 and 30 eV at different sample temperatures in the region m/e = 0–50. With the detection of hydrogen indicated by a m/e = 2 peak, the intensity as a function of time for masses m/e = 1, m/e = 2, m/e = 3, m/e = 4, m/e = 5, and m/e = 18 was obtained while changing the ionization potential (IP) of the mass spectrometer from 30 to 70 eV.

The control hydrogen gas was ultrahigh purity (MG Industries).

3. Results and discussion

3.1. ToF-SIMS

3.1.1. ToF-SIMS of potassium iodo hydride sample

The positive ToF-SIMS spectrum (m/e = 0–140) of KHI, the positive ToF-SIMS spectrum (m/e = 0–140) of KI, the negative ToF-SIMS spectrum (m/e = 0–140) of KHI, and

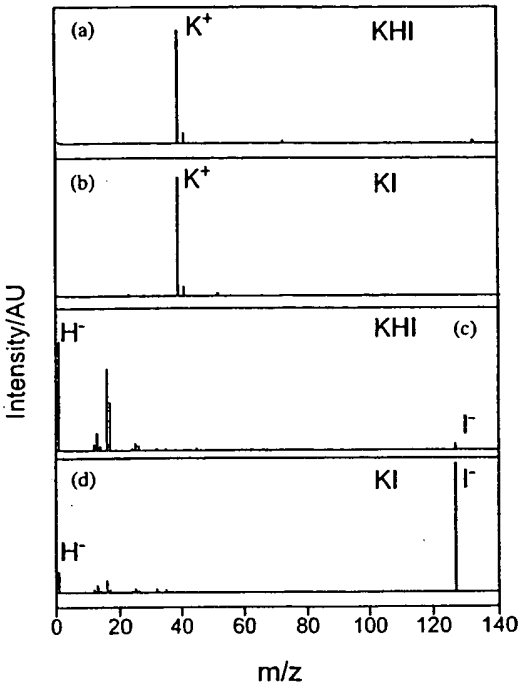

Fig. 3. (a) The positive ToF-SIMS spectrum (m/e = 0–140) of KHI. (b) The positive ToF-SIMS spectrum (m/e = 0–140) of KI. (c) The negative ToF-SIMS spectrum (m/e = 0–140) of KHI. (d) The negative ToF-SIMS spectrum (m/e = 0–140) of KI.

the negative ToF-SIMS spectrum (m/e = 0–140) of KI are shown in Figs. 3a–d, respectively. The positive ion spectrum of KHI and that of the KI control were dominated by the K^+ ion. A K^{2+} ion was only observed in the positive ion spectrum of the KHI.

Ga^+ m/z = 69, K_2^+ m/z = 78, $K(KCl)^+$ m/z = (113), I^+ m/z = 127, KI^+ m/z = 166, and a series of positive ions $K[KI]_n^+$ m/z = (39 + 166n) were also observed. The negative ion ToF-SIMS of KHI was dominated by H^- with a smaller I^- peak. Iodide alone dominated the negative ion ToF-SIMS of the KI control. For both, O^- m/z = 16, OH^- m/z = 17, Cl^- m/z = 35, KI^- m/z = 166, a series of negative ions $I[KI]_n^-$ m/z = (127 + 166n) were also observed.

3.1.2. ToF-SIMS of potassium hydride potassium hydrogen carbonate sample

The positive ToF-SIMS spectrum obtained from the $KHCO_3$ control is shown in Figs. 4 and 5. ($KHCO_3$ was used as a control versus K_2CO_3 because the former is more conservative in that it contains a larger source of H). In addition, the positive ToF-SIMS of the KH $KHCO_3$ sample is shown in Figs. 6 and 7. In both the control and KH $KHCO_3$ samples, the positive ion spectrum are dominated by the K^+ ion. Two series of positive ions $\{K[K_2CO_3]_n^+$ m/z = (39 + 138n) and $K_2OH[K_2CO_3]_n^+$ m/z = (95 + 138n)$\}$ are observed in the $KHCO_3$ control. Other peaks containing potassium include KC^+, $K_xO_y^+$, $K_xO_yH_z^+$, KCO^+, and K_2^+. However, in the KH $KHCO_3$ sample, three new series of positive ions are observed at $\{K[KH\,KHCO_3]_n^+$ m/z = (39 + 140n), $K_2OH[KH\,KHCO_3]_n^+$ m/z = (95 + 140n), and $K_3O[KH\,KHCO_3]_n^+$ m/z = (133 + 140n)$\}$. These ions correspond to inorganic clusters containing novel hydride combinations (i.e. KH $KHCO_3$ units plus other positive fragments). The same compound was seen previously in a sample isolated from a K_2CO_3 electrolytic cell [9].

The comparison of the positive ToF-SIMS spectrum of the $KHCO_3$ control with the KH $KHCO_3$ sample shown in Figs. 4 to 5 and 6, 7, respectively, demonstrates that the $^{39}K^+$ peak of the KH $KHCO_3$ sample may saturate the detector and give rise to a peak that is atypical of the natural abundance of ^{41}K. The natural abundance of ^{41}K is 6.7%; whereas, the observed ^{41}K abundance from the KH $KHCO_3$ sample is 53%. The high resolution mass assignment of the m/z = 41 peak of the KH $KHCO_3$ was consistent with ^{41}K, and no peak was observed at m/z = 42.98 ruling out KH_2^+. Moreover, the natural abundance of ^{41}K was observed in the positive ToF-SIMS spectra of $KHCO_3$, KNO_3, and KI standards that were obtained with an ion current such that the ^{39}K peak intensity was an order of magnitude higher than that given for the KH $KHCO_3$ sample. The saturation of the ^{39}K peak of the positive ToF-SIMS spectrum by the KH $KHCO_3$ sample is indicative of a unique crystalline matrix [10].

The negative ToF-SIMS spectrum (m/e = 0–100) of the $KHCO_3$ (99.99%) sample and the KH $KHCO_3$ sample are shown in Figs. 8 and 9, respectively. The negative ion ToF-SIMS of the KH $KHCO_3$ sample was dominated by H^-, O^-, and OH^- peaks. A series of nonhydride containing negative ions $\{KCO_3[K_2CO_3]_n^-$ m/z = (99 + 138n)$\}$ was also present which implies that H_2 was eliminated from KH $KHCO_3$ during fragmentation of the compound KH $KHCO_3$. Comparing the H^- to O^- ratio of the KH $KHCO_3$ sample to that of the $KHCO_3$ control sample, the H^- peak was about an order of magnitude higher in the KH $KHCO_3$ sample.

3.1.3. ToF-SIMS of rubidium fluoro hydride sample

The positive ToF-SIMS spectrum (m/e = 0–100) of RbHF, the positive ToF-SIMS spectrum (m/e = 0–100) of RbF, the negative ToF-SIMS spectrum (m/e = 0–100) of RbHF, and the negative ToF-SIMS spectrum (m/e = 0–100) of RbF are shown in Figs. 10a–d, respectively. The positive ion spectrum of RbHF and that of the RbF control were dominated by the Rb^+ ion. Ga^+ m/z = 69, Rb_2^+ m/z = 170, RbF^+ m/z = 104, and a series of positive ions $Rb[RbF]_n^+$ m/z = (85 + 104n) were also observed. The negative ion ToF-SIMS of RbHF was dominated by H^- with a smaller F^- peak. Fluorine alone dominated the negative ion ToF-SIMS of the RbF control. For both, O^- m/z = 16, OH^- m/z = 17, Cl^- m/z = 35, RbF^- m/z = 104, a series of negative ions $F[RbF]_n^-$ m/z = (19 + 104n) were also observed.

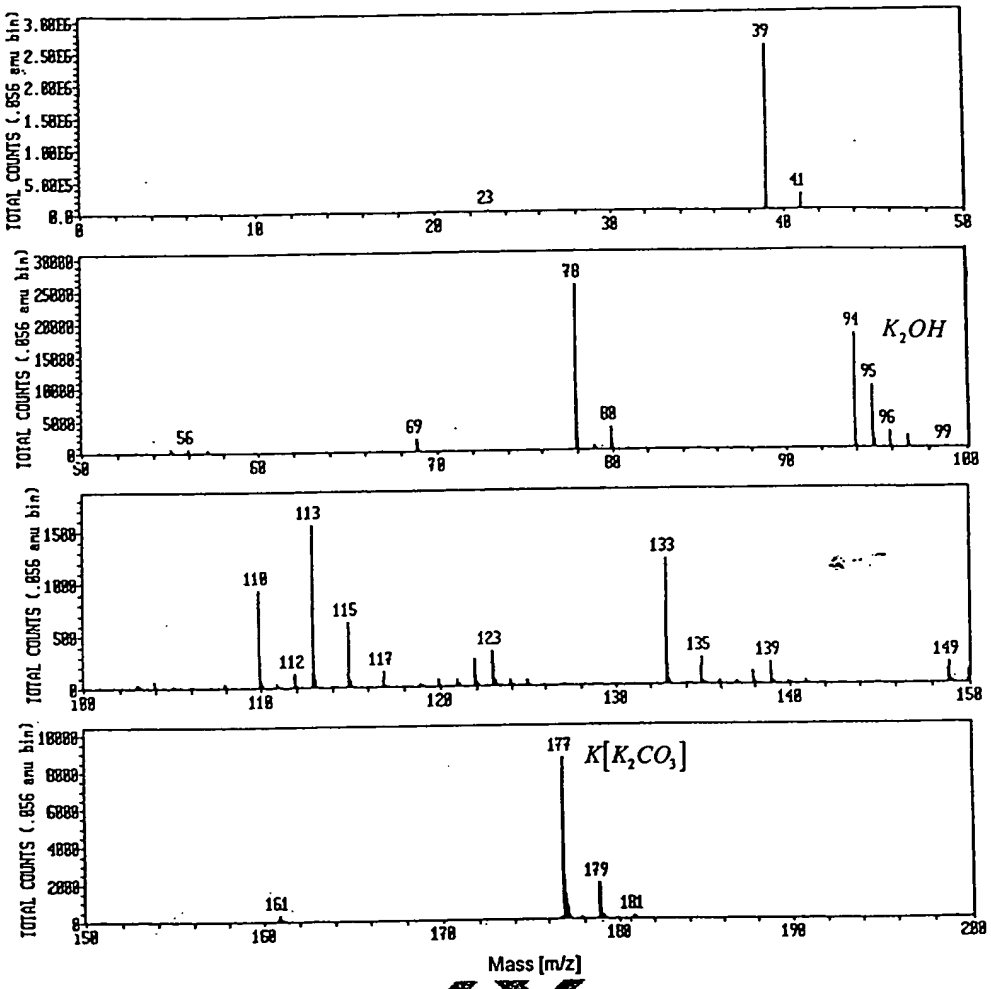

Fig. 4. The positive ToF-SIMS spectrum (m/z = 0–200) of $KHCO_3$ (99.99%) where HC = hydrocarbon.

3.1.4. ToF-SIMS of strontium fluoro hydride sample

The positive ToF-SIMS spectrum obtained from the SrHF sample is shown in Fig. 11. The positive spectrum was dominated by the strontium peaks Sr^+ m/z = 88 and a $^{88}SrH^+$ m/z = 89 peak. Lithium, sodium, potassium, small hydrocarbon fragments such as C_2H_3 m/z = 27 and C_2H_5 m/z = 29, $^{48}Ti^+$ m/z = 48, $^{48}TiH^+$ m/z = 49, $Ti_xO_y^+$, $Ti_xO_yH^+$, K_2F^+ m/z = 97 $^{88}SrOH^+$ m/z = 105, $^{88}SrF^+$ m/z = 107 were also observed.

The positive spectrum of the SrF_2 control was also dominated by the by the strontium peak Sr^+ m/z = 88. A much smaller $^{88}SrH^+$ m/z = 89 peak was present. Lithium, sodium, potassium, hydrocarbon fragments, $^{88}SrOH^+$ m/z = 105, $^{88}SrF^+$ m/z = 107 were also observed. The hydrocarbon peaks were much more intense in the control sample than in the SrHF sample, and a large silicon peak was present.

The negative ion ToF-SIMS of SrHF shown in Fig. 12 was dominated by H^- and F^- m/z = 19 of equal intensity. Fluoride alone dominated the negative ion ToF-SIMS of the SrF_2 control. For both samples, smaller O^- m/z = 16, OH^- m/z = 17, hydrocarbon fragment peaks such as C^- m/z=12 and CH^- m/z=13, Cl^- m/z=35, SrF_2^- m/z= 126, and I^- m/z=127 were observed. A hydride peak which was significantly smaller than the O^- m/z = 16 peak was observed in the control. $Ti_xO_yH^-$ was observed in the SrHF sample. The hydrocarbon peaks were much more intense in the control.

The negative ToF-SIMS relative sensitivity factors (RSF) for the halides are all about equivalent. The hydrino hydride ion is in the same group as the halide ions. Thus, its RSF is projected to be equivalent to that of the halides. Therefore, the atomic percentage of hydrino hydride ion may be determined by comparison of its intensity with that of the fluoride ion of the product SrHF. The atomic percentage of hydrino hydride ion is equivalent to that of fluoride as shown in the negative ToF- SIMS. Since essentially no other cations are present, the positive and negative ToF-SIMS

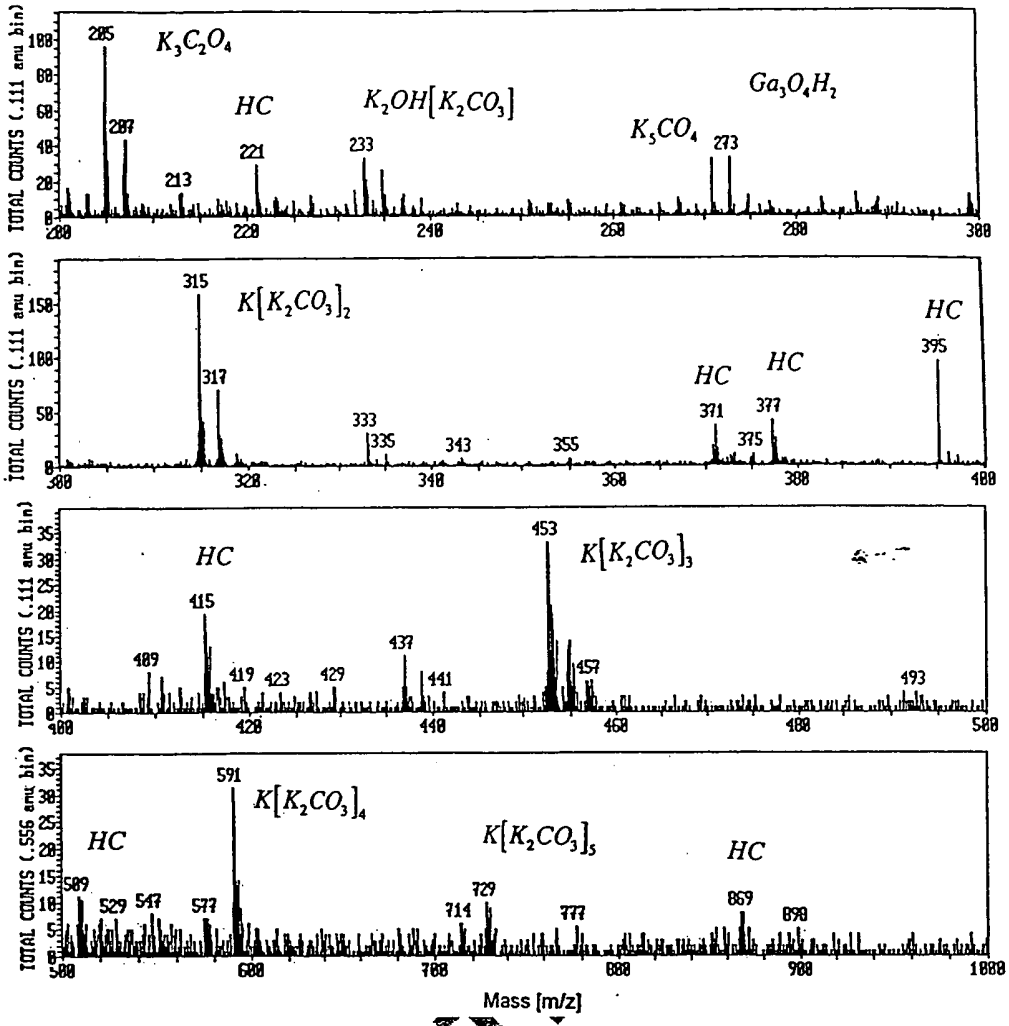

Fig. 5. The positive ToF-SIMS spectrum (m/e = 200–1000) of $KHCO_3$ (99.99%) where HC = hydrocarbon.

indicates that SrHF is the product of the gas cell reaction of SrF_2 in the presence of atomic hydrogen and strontium metal catalyst.

3.2. XPS

3.2.1. XPS of potassium iodo hydride sample

A survey spectrum was obtained over the region $E_b = 0$ to 1200 eV. The primary element peaks allowed for the determination of all of the elements present in MHX and the control MX. The survey spectrum also detected shifts in the binding energies of the elements which had implications to the identity of the compound containing the elements.

The XPS survey scan of KI and KHI are shown in Figs. 13a and b, respectively. C1s at 284.5 eV was used as the internal standard for KHI and the control KI. The major species present in the KHI sample and the control are potassium and iodide. Trace small amounts of carbonate carbon and oxygen were also identified in the KHI sample.

The 0–100 eV binding energy region of a high resolution XPS spectrum of KI and KHI are shown in Figs. 14a and b, respectively. Peaks centered at 21 and 37 eV which do not correspond to any other primary element peaks were observed in the case of the KHI sample. The intensity and shift match shifted K3 s and K3 p. Hydrogen is the only element which does not have primary element peaks; thus, it is the only candidate to produce the shifted peaks. These peaks may be shifted by a highly binding hydride ion $H^-(1/6)$ with a binding energy of 22.8 eV given by Eq. (A.12) that bonds to potassium K3 p and shifts the peak to this energy. In this case, the K3 s is similarly shifted.

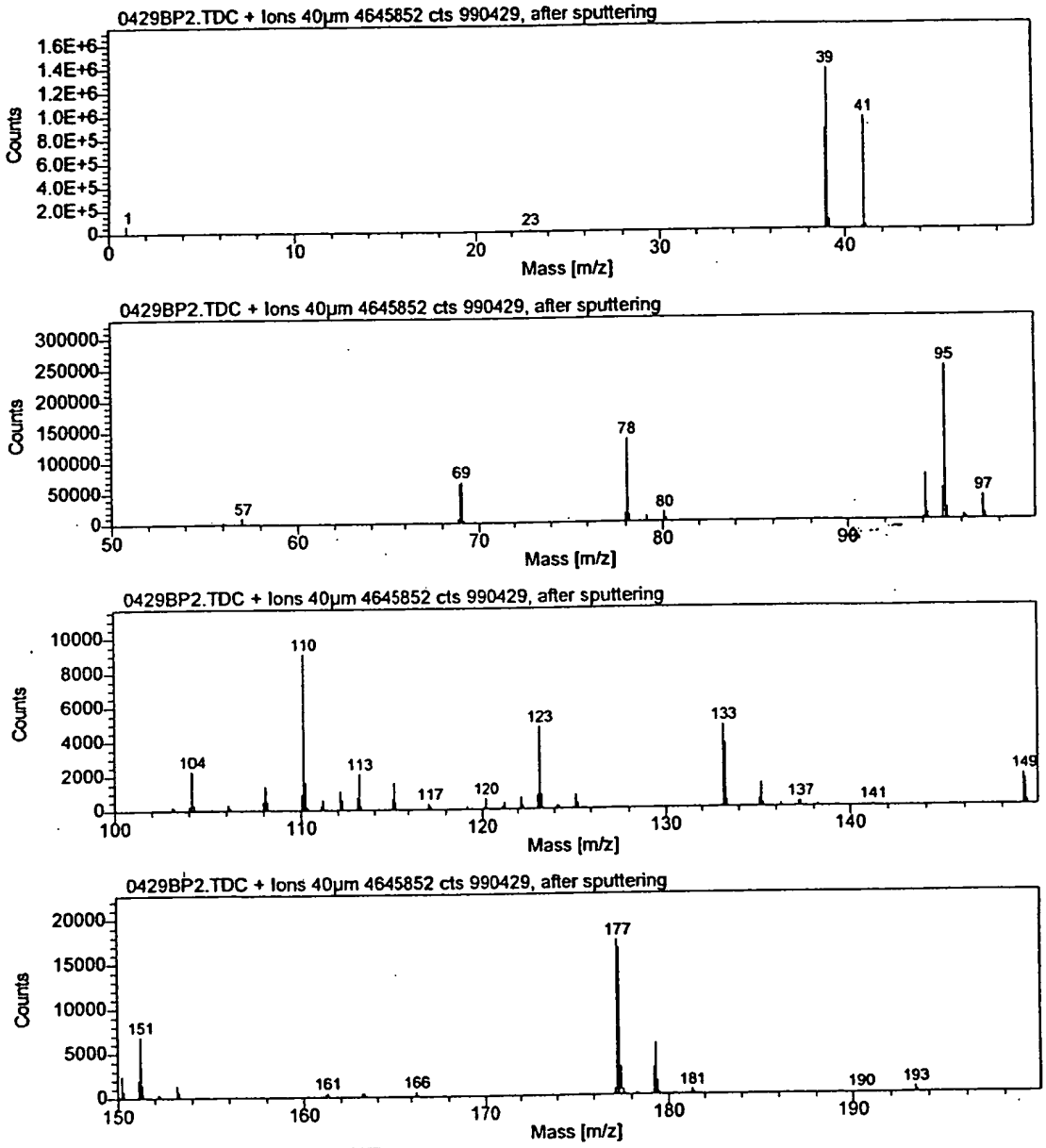

Fig. 6. The positive ToF-SIMS spectrum ($m/e = 0$–200) of the KH $KHCO_3$ sample.

3.2.2. *XPS of potassium chloro hydride sample*

A survey spectrum was obtained over the region $E_b = 0$ to 1200 eV. The primary element peaks allowed for the determination of all of the elements present in the magenta crystals of the KHCl sample and the control KCl. The survey spectrum also detected shifts in the binding energies of the elements which had implications to the identity of the compound containing the elements.

The XPS survey scan of the KHCl sample and the KCl control sample are shown in Figs. 15 and 16, respectively. Cls at 284.6 eV was used as the internal standard for the KHCl sample and the control KCl sample. The major species observed in the KHCl sample and the control were potassium and chlorine. Trace small amounts of carbon, oxygen, fluorine, iodine, and silicon were also identified in the KHCl sample. The identifying peaks of the primary elements and their binding energies are: $FKL_{23}L_{23}$ at 831.0 eV, F1s at 688.4 eV and at 682.8 eV, O1s at 530.6 eV, K2s at 377.2 eV, $K2p_{1/2}$ at 295.4 eV, $K2p_{3/2}$ at 292.5 V, C1s at 284.6 eV, Cl2s at 268.9 eV, $Cl2p_{1/2}$ at 199.5 eV, $Cl2p_{3/2}$ at 198.0 eV, Si2s at 152.4 eV, and $Si2p_{3/2}$ at 101.9 eV. The K 3p and K 3s of the KHCl sample occurred at 16.7 and 32.8 eV,

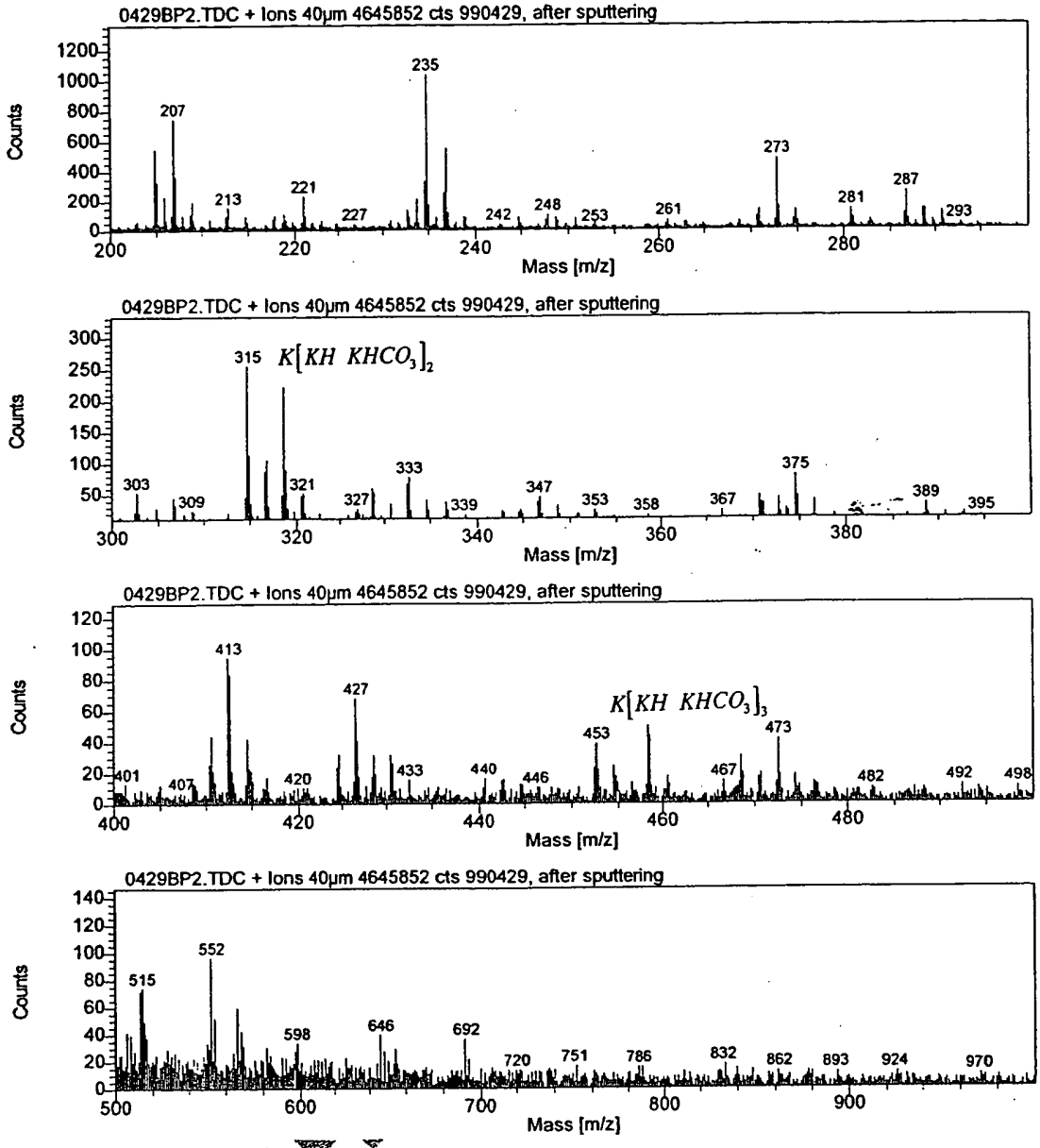

Fig. 7. The positive ToF-SIMS spectrum ($m/e = 200–1000$) of the KH $KHCO_3$ sample.

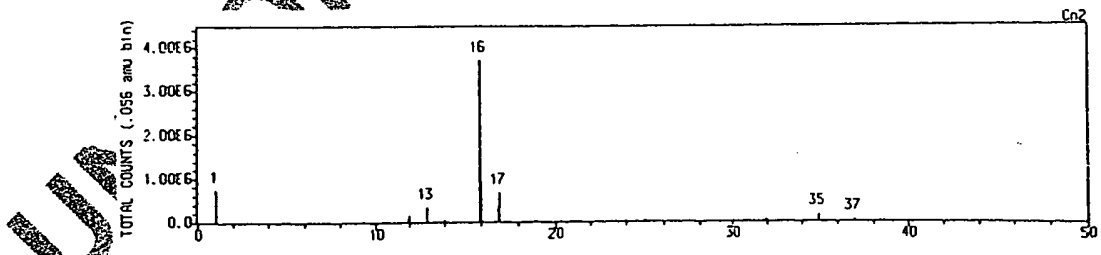

Fig. 8. The negative ToF-SIMS spectrum ($m/e = 0–100$) of the $KHCO_3$ (99.99%) sample.

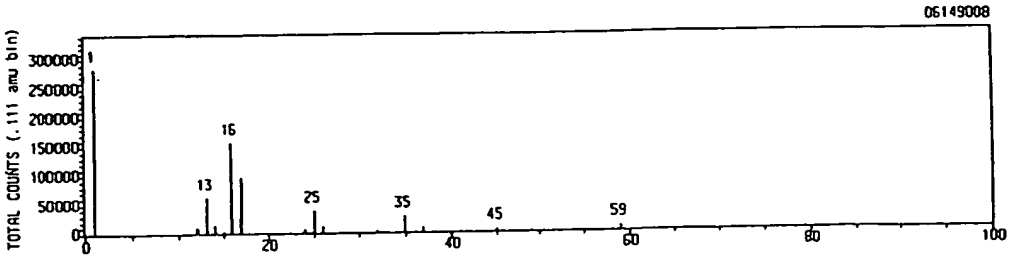

Fig. 9. The negative ToF-SIMS spectrum ($m/e = 0$–100) of the KH $KHCO_3$ sample.

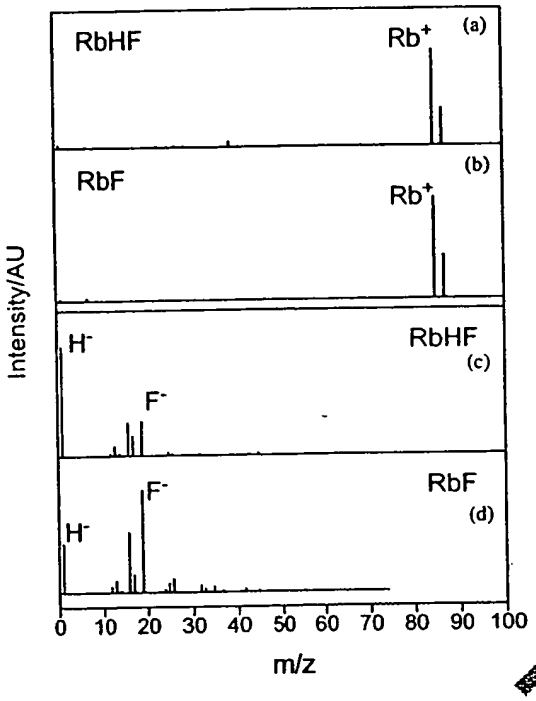

Fig. 10. (a) The positive ToF-SIMS spectrum ($m/e = 0$–100) of RbHF. (b) The positive ToF-SIMS spectrum (m/e=0–100) of RbF. (c) The negative ToF-SIMS spectrum ($m/e = 0$–100) of RbHF. (d) The negative ToF-SIMS spectrum ($m/e = 0$–100) of RbF.

respectively. The K3p and K3 s of the control KCl occurred at 17.0 and 32.8 eV, respectively.

No elements were present in the survey scan which could be assigned to peaks in the low binding energy region with the exception of the K 3p and K 3s peaks at 16.7 and 32.8 eV, respectively, and the $I4d_{3/2}$ and $I4d_{5/2}$ peaks at 51.8 and 49.7 eV respectively. Accordingly, any other peaks in this region must be due to novel species. The 0–125 eV binding energy region of a high resolution XPS spectrum of the KHCl sample and the control KCl sample are shown in Figs. 17 and 18, respectively. The XPS spectrum of the KHCl sample differs from that of KCl by having an additional feature at 36.7 eV. The XPS peak centered at 36.7 eV that does not correspond to any other primary element peak may correspond to the $H^-(n = 1/8)E_b = 36.1$ eV hydride ion given by Eq. (A.12) where E_b is the predicted vacuum binding energy. Also the K3s and K3 p peaks in the KHCl sample are wider when compared to the K3 s and K3 p of the KCl control. The Cl3p at 16 eV is merged with the K3 p of the KHCl sample, but the peaks are separated in the control taken at the same resolution. This clearly indicates that the environment of K in the KHCl sample is different from that of KCl. The data further indicates the formation of a novel compound.

3.2.3. *XPS of alkali halido hydrides and alkaline earth halido hydrides samples*

The binding energies and features of core level electrons of a series of alkali and alkaline earth halido hydrides (KHF, KHCl, KHBr, KHI, RbHF, RbHCl, RbHBr, RbHI, CsHF, CsHCl, CsHBr, CsHI, CaHCl, CaHBr, CaHI, SrHF, SrHCl, and SrHBr) were analyzed by XPS. The local structure of metal halides and metal halido hydrides was investigated by studying the metal core levels including K 2p, Rb 3d, Cs 3d, Ca 2p, and Sr 3d, and halogen core level including F 1s, Cl 2p Br 2p, and I 3d. As atomic hydrogen undergoes reaction with a catalyst to form a lower-energy hydrogen species which subsequently reacts with the metal center in a halide compound, alterations in the electronic structure of the metal such as changes in core level binding energies and spin-orbital energies relative to the starting halide are expected. In order to compare the full width at half maximum (FWHM) of the peaks, the difference between spin-orbit splitting in the core level was determined using curve fitting in the same or a close energy range. In some cases, the absolute core level binding energy was not calibrated, which did not affect the validity of the comparison of FWHM values. The results of the determination of the binding energies of selected core level electrons, full width at half maximum of the peaks, and energy of spin-orbital splitting for alkali halido hydrides, calcium halido hydrides, and strontium halido hydrides compared with the corresponding alkali halides, calcium halides, and strontium halides are listed in Tables 1–3, respectively. The XPS spectra of the K 2p core level in KI, KHI appear in Figs. 19a and b, respectively. The XPS spectra of the I 3d core level in KI and KHI appear in Figs. 20a and b, respectively. The XPS spectra of the Ca 2p core level in $CaBr_2$ and CaHBr appear in Figs. 21a and

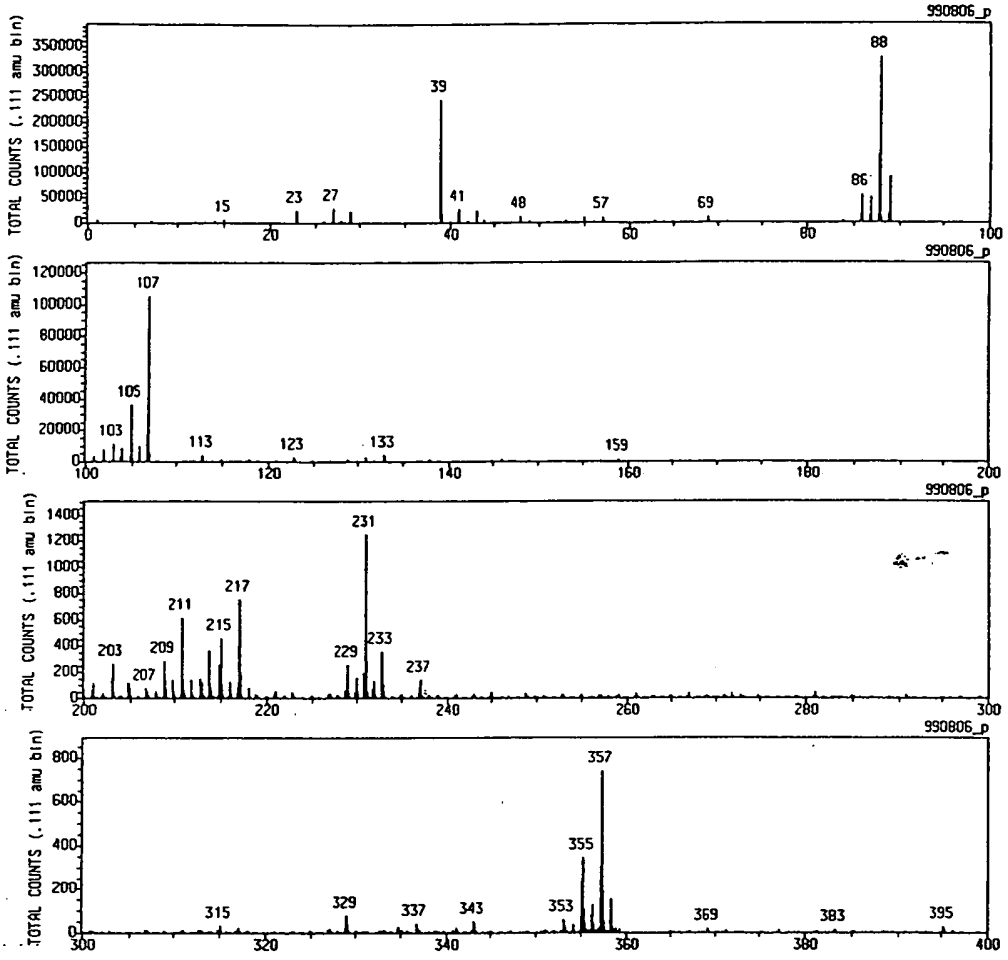

FILE NAME: 990806_p DATE : 19 Aug 99 8:14 ACQUISITION TIME: 10.0 MIN. SPECTRUM INTEGRAL : 1632750
990806_p1;
+ IONS PRIMARY GUN: LMIG TIME RECORDER: Multi-Stop TDC X-Y SOURCE: Raster TIME PER CHANNEL: 138 ps
DATA SET: 0 Spectra; 0 Image(s) RASTER SIZE: 81μm RASTER TYPE: 81

Fig. 11. The positive ToF-SIMS spectrum obtained from the SrHF sample.

b, respectively. The XPS spectra of the Sr 3d core level in $SrBr_2$ and SrHBr appear in Figs. 22a and b, respectively. The XPS spectra of the Br 2p core level in $SrBr_2$ and SrHBr appear in Figs. 23a and b, respectively.

It is clear that the FWHM of the metal core level peaks in alkali and alkaline earth halido hydrides is broader than that in the corresponding halides. The magnitude of broadening ranges from 0.3 to 0.9 eV, depending on compound. The trend for the broadening effect follows the sequence: iodo hydrides > bromo hydrides > fluoro hydrides~chloro hydrides. In contrast, the halogen core level FWHM in both alkali and alkaline earth halido hydrides is broadened by only about 0.2 to 0.3 eV compared to the corresponding halide. Comparing the alterations in the metal core levels versus the halogen core level indicates that the lower-energy hydrogen species is bound to the metal center of the alkali or alkaline earth halide. This binding influences the metal core level with little perturbation of the halogen core level.

Each of the spectra of potassium iodo hydride, calcium bromo hydride, and strontium bromo hydride were curve fit with one spin-orbit splitting component having a similar FWHM and energy separation as that of the starting material potassium iodide, calcium bromide, and strontium bromide, respectively. An additional spin-orbit splitting component had to be added to each of potassium iodo hydride, calcium bromo hydride, and strontium bromo hydride in order to obtain a good curve fit of the K 2p, Ca 2p, and Sr 3d spectra. In each case, the second component of spin-orbit splitting is assigned to the formation of the alkali or

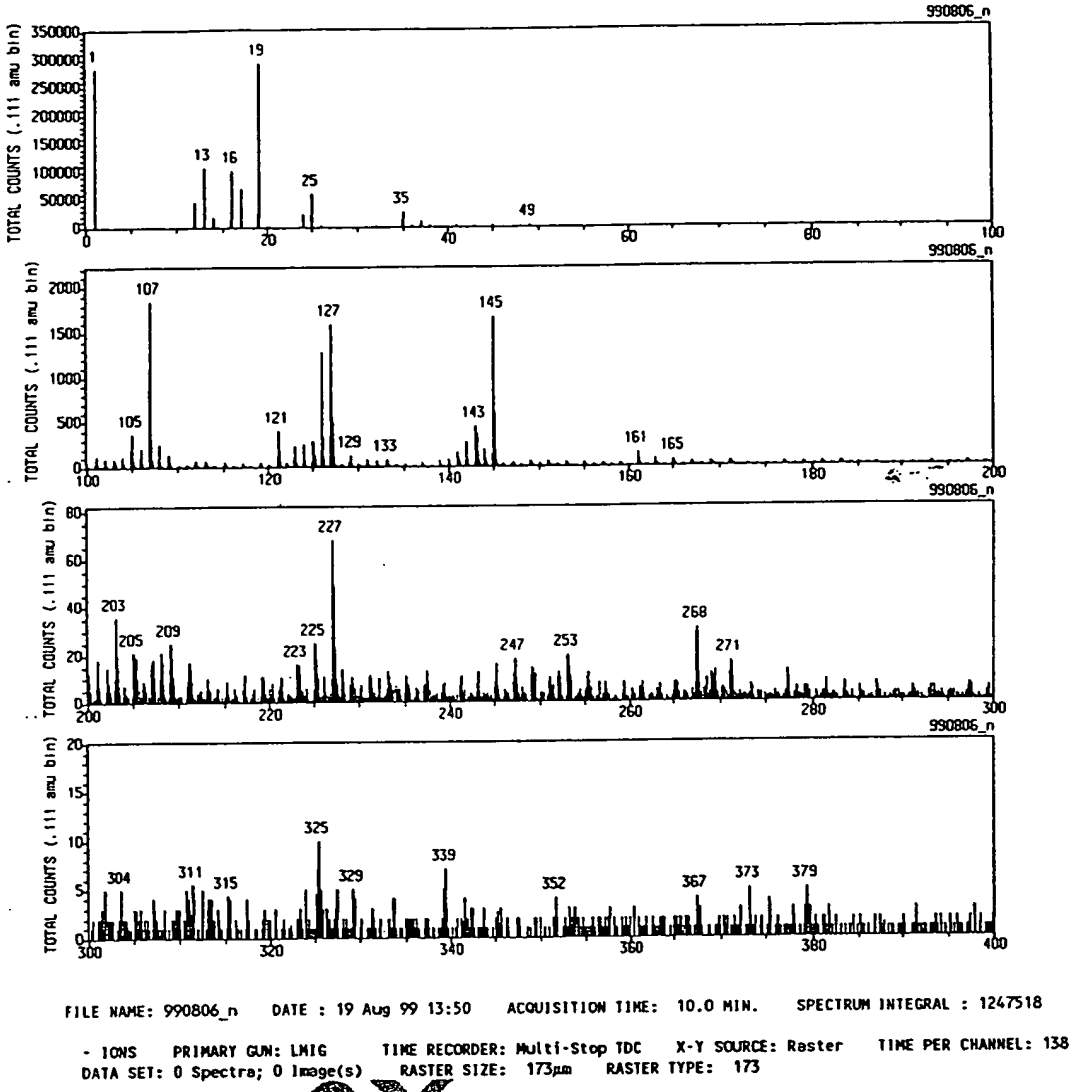

Fig. 12. The negative ToF-SIMS spectrum obtained from the SrHF sample.

alkaline earth metal halido hydride, KHI, CaHBr, and SrHBr, respectively. The presence of the novel hydride ion shifts the K 2p, Ca 2p, and Sr 3d peaks to lower binding energies relative to the corresponding peaks of KI, $CaBr_2$, and $SrBr_2$, respectively.

The XPS data clearly indicates a change in the electronic structure at the metal core level and different bonding in the metal halide hydrides relative to that in the corresponding metal halides. It strongly suggests the formation of a novel metal hydride which is consistent with the supporting data provided by XPS given above and NMR, ToF-SIMS, and gas chromatography/mass spectroscopy given in the respective sections.

3.3. NMR

To eliminate the possibility that the alkali halide MX influenced the local environment of the ordinary alkali hydride MH to produce an NMR resonance that was shifted upfield relative to MH alone, controls comprising MH and a MH/MX mixture were run.

3.3.1. NMR of potassium iodo hydride sample

The ^1H MAS NMR spectra of the KHI sample, the control comprising an equal molar mixture of KH and KI, and control KH relative to external tetramethylsilane (TMS) are shown in Figs. 24a, b, and c, respectively. Ordinary hy-

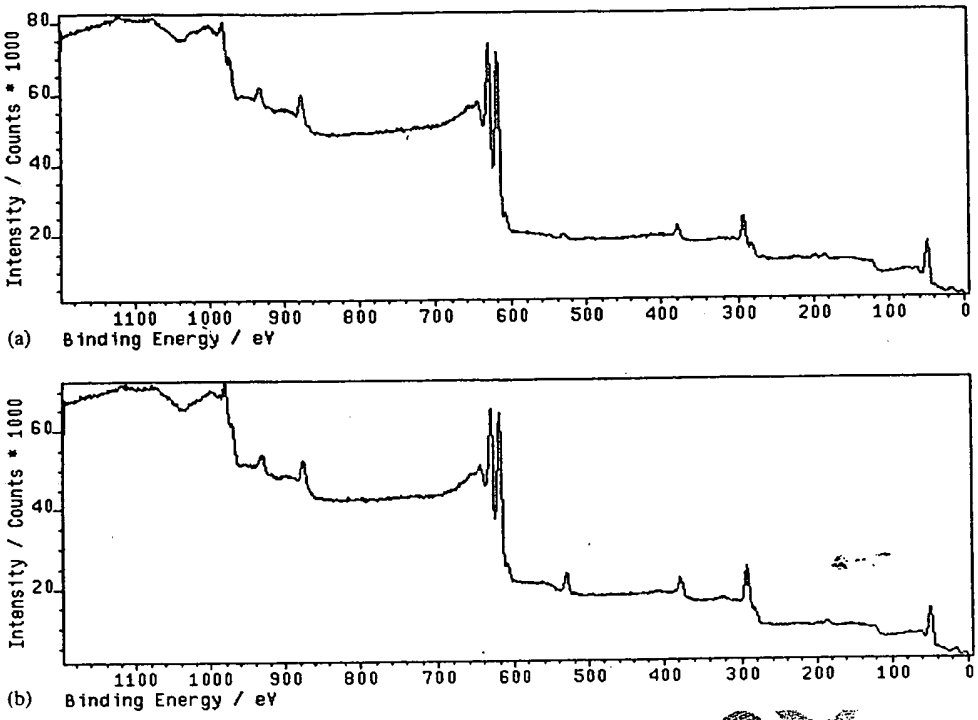

Fig. 13. (a) The XPS survey scan of KI. (b) The XPS survey scan of KHI.

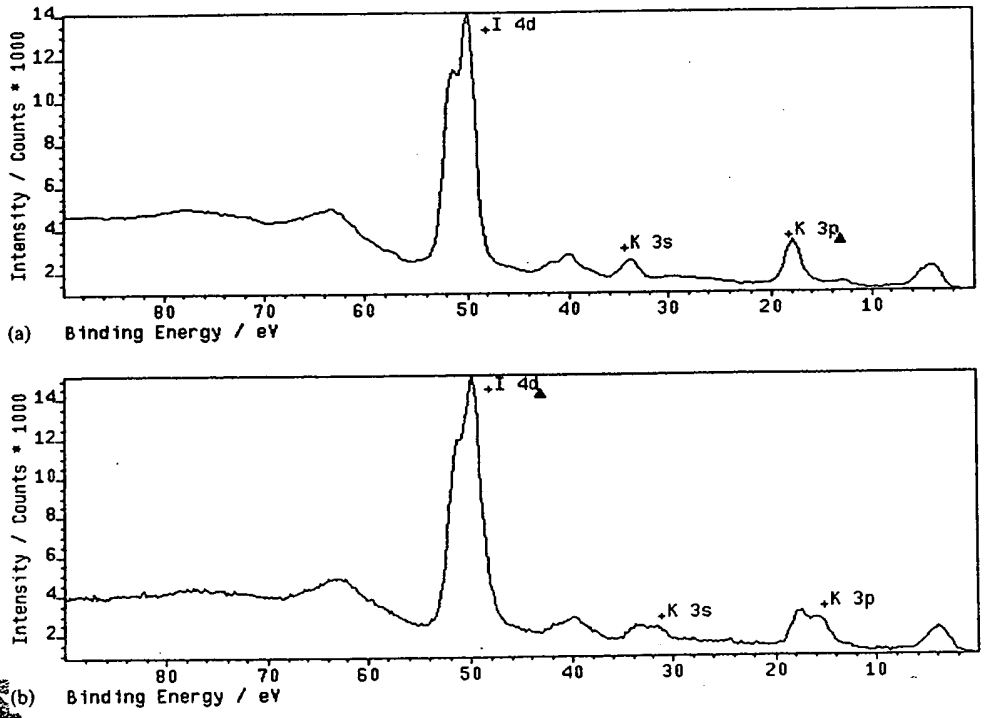

Fig. 14. (a) The 0–100 eV binding energy region XPS spectrum of KI. (b) The 0–100 eV binding energy region XPS spectrum of KHI.

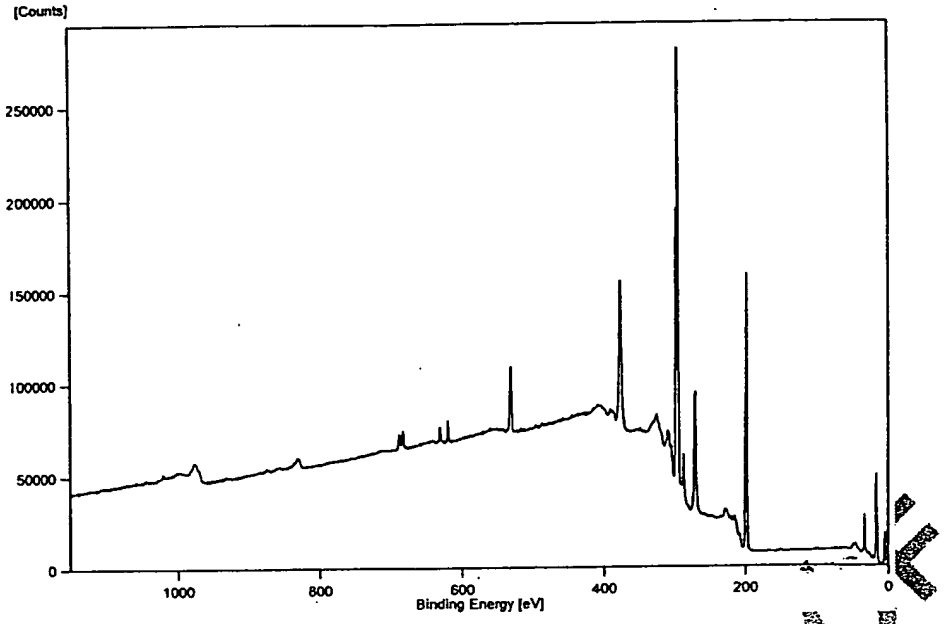

Fig. 15. The XPS survey scan of the KHCl sample.

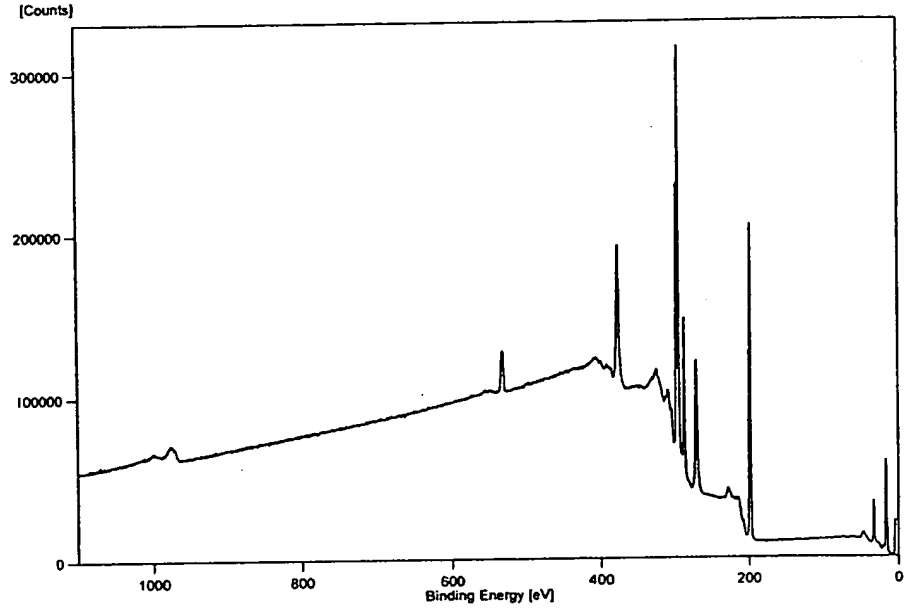

Fig. 16. The XPS survey scan of the KCl control sample.

dride ion has a resonance at 1.1 and 0.8 ppm in the KH/KI mixture and in KH alone as shown in Figs. 24b and c, respectively. The additional peak at 4.5–4.6 ppm is assigned to KOH formed from air exposure of KH during sample handling. The spin speed was varied to confirm real peaks versus side bands. The latter changed position with spin speed, the former were independent of spin speed. The unlabeled peaks shown in Figure 24a were found to be sidebands.

The presence of KI does not shift the resonance of ordinary hydride. The resonance at 0.9 ppm which is assigned to ordinary hydride ion was observed in the spectrum of the KHI sample as shown in Fig. 24a. The distinct 0.8 and 1.1 ppm resonances could not be resolved if they were present.

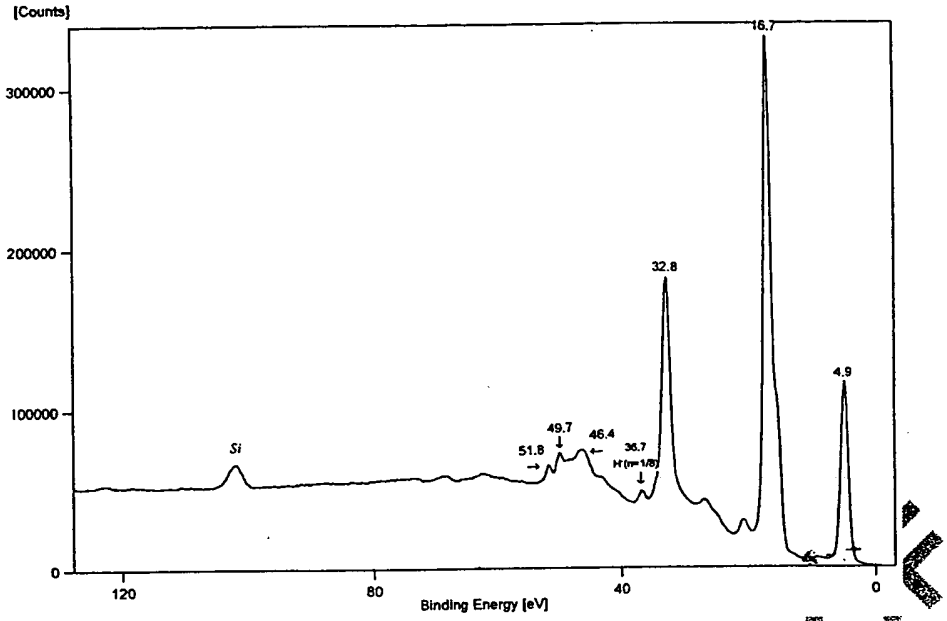

Fig. 17. The 0–125 eV binding energy region of a high resolution XPS spectrum of the KHCl sample.

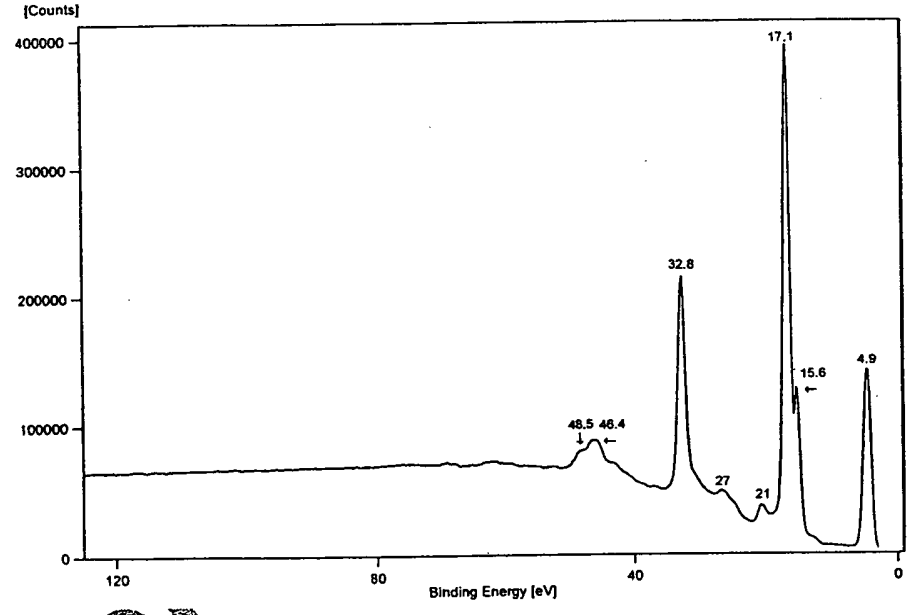

Fig. 18. The 0–125 eV binding energy region of a high resolution XPS spectrum of the KCl control sample.

A large distinct upfield resonance was observed at −3.2 ppm which was not observed in either control. This upfield shifted peak is consistent with a hydride ion with a smaller radius as compared with ordinary hydride since a smaller radius increases the shielding or diamagnetism. The −3.2 ppm peak is assigned to a novel hydride ion that has a smaller radius than that of ordinary hydride ion since the shift was extraordinarily far upfield in the case of the KHI sample.

3.3.2. *NMR of potassium chloro hydride sample*

The ^{1}H MAS NMR spectra of the KHCl sample, the control comprising an equal molar mixture of KH and KCl, and the control KH relative to external tetramethylsilane (TMS) are shown in Figs. 25a, b, and c, respectively. Ordinary hydride ion has a resonance at 1.1 and 0.8 ppm in the KH/KCl mixture and in KH alone as shown in Figs. 25b and c, respectively. The additional peak at 6 ppm is assigned

Table 1
The results of the determination of the binding energies of selected core level electrons, full width at half maximum of the peaks, and energy of spin-orbit splitting for alkali halido hydrides compared with the corresponding alkali halides

Compound	Peak	Binding energy (eV)[a]	Full width at half maximum (FWHM) (eV)	Energy of spin-orbit splitting (eV)
KF	K 2p3/2	298.37	2.24	2.80
	K 2p1/2	301.11	2.27	
	F 1s	688.97	2.33	
KHF	K 2p3/2	296.12	2.61	2.72
	K 2p1/2	298.84	2.61	
	F 1s	687.60	2.20	
KCl	K 2p3/2	296.87	1.88	2.75
	K 2p1/2	299.62	1.97	
	Cl 2p3/2	202.27	1.82	1.68
	Cl 2p1/2	203.95	1.58	
KHCl	K 2p3/2	297.09	1.91	2.76
	K 2p1/2	299.85	1.98	
	Cl 2p3/2	202.57	1.77	1.62
	Cl 2p1/2	204.19	1.60	
KBr	K 2p3/2	297.15	1.63	2.75
	K 2p1/2	299.90	1.72	
	Br 3p3/2	186.34	2.55	6.87
	Br 3p1/2	193.07	2.39	
KHBr	K 2p3/2	296.90	2.10	2.76
	K 2p1/2	299.66	1.86	
	Br 3p3/2	186.18	2.53	6.79
	Br 3p1/2	192.87	1.99	
KI	K $2p_{3/2}$	294.44	1.84	2.75
	K $2p_{1/2}$	297.19	1.9[illegible]	
	I $3d_{3/2}$	620.37	2.07	11.53
	I $3d_{3/2}$	631.90	2.14	
KHI	K $2p_{3/2}$	294.37	1.83	2.77
	K $2p_{1/2}$	297.14	1.81	
	K $2p_{3/2}$	292.51	1.87	3.00
	K $2p_{1/2}$	295.51	1.78	
	I $3d_{5/2}$	621.08	2.17	11.52
	I $3d_{3/2}$	632.60	2.20	
RbF	Rb $3d_{5/2}$	115.00	2.28	1.55
	Rb $3d_{3/2}$	116.55	2.08	
	F 1s	688.35	2.30	
RbHF	Rb $3d_{5/2}$	114.65	1.95	1.55
	Rb $3d_{3/2}$	116.37	1.56	
	Rb $3d_{5/2}$	114.02	2.24	1.56
	Rb $3d_{3/2}$	115.58	1.88	
	F 1s	688.35	2.10	
RbCl	Rb $3d_{5/2}$	115.17	1.84	1.55
	Rb $3d_{3/2}$	116.72	1.77	

Table 1. (Continued)

Compound	Peak	Binding energy (eV)[a]	Full width at half maximum (FWHM) (eV)	Energy of spin-orbit splitting (eV)
	Cl $2p_{3/2}$	203.39	1.75	1.66
	Cl $2p_{1/2}$	205.05	1.69	
RbHCl	Rb $3d_{5/2}$	114.30	2.17	1.56
	Rb $3d_{3/2}$	115.86	2.02	
	Cl $2p_{3/2}$	202.59	2.01	1.72
	Cl $2p_{1/2}$	204.33	1.70	
RbBr	Rb $3d_{5/2}$	114.46	1.76	1.51
	Rb $3d_{3/2}$	115.97	1.83	
	Br $3p_{3/2}$	186.56	2.88	6.66
	Br $3p_{1/2}$	193.22	1.75	
RbHBr	Rb $3d_{5/2}$	114.54	1.74	1.56
	Rb $3d_{3/2}$	116.0	1.85	
	Br $3p_{3/2}$	186.65	2.70	6.63
	Br $3p_{1/2}$	193.38	1.69	
RbI	Rb $3d_{5/2}$	114.54	1.99	1.55
	Rb $3d_{3/2}$	116.09	1.81	
	I $3d_{5/2}$	623.72	2.04	11.49
	I $3d_{3/2}$	635.21	2.07	
RbHI	Rb $3d_{5/2}$	114.29	2.31	1.56
	Rb $3d_{3/2}$	115.85	1.89	
	I $3d_{5/2}$	623.28	2.10	11.50
	I $3d_{3/2}$	634.78	2.17	
CsF	Cs $3d_{5/2}$	746.18	2.26	
	F 1s	690.55		
CsHF	Cs $3d_{5/2}$	741.30	2.2	
	Cs $3d_{5/2}$	738.63	2.19	
	F 1s	687.81	3.01	
	F 1s	684.23	2.60	
CsCl	Cs $3d_{5/2}$	74[illegible]71	2.04	
	Cl $2p_{3/2}$	205.18	1.65	1.50
	Cl $2p_{1/2}$	206.78	1.43	
CsHCl	Cs $3d_{5/2}$	738.57	2.35	
	Cl $2p_{3/2}$	203.60	1.73	1.56
	Cl $2p_{1/2}$	205.24	1.58	
CsBr	Cs $3d_{5/2}$	745.01	1.78	
	Cs $3d_{3/2}$			
	Br $2p_{3/2}$	188.33	2.35	6.68
	Br $2p_{1/2}$	195.01	2.13	
CsHBr	Cs $3d_{5/2}$	728.79	2.40	
	Cs $3d_{3/2}$			
	Br $2p_{3/2}$	186.38	2.45	6.63
	Br $2p_{1/2}$	193.01	2.08	

[a] Uncalibrated, except for KI and KHI.

Table 2
The results of the determination of binding energies of selected core level electrons, full width at half maximum of the peaks, and energy of spin-orbit splitting for calcium halido hydrides compared with the corresponding calcium halides

Compound	Peak	Binding energy (eV)[a]	Full width at Half Maximum (FWHM) (eV)	Energy of spin-orbit splitting (eV)
$CaCl_2$	Ca $2p_{3/2}$	352.18	2.25	3.51
	Ca $2p_{1/2}$	355.69	2.19	
	Cl $2p_{3/2}$	203.12	2.28	1.81
	Cl $2p_{1/2}$	204.93	1.86	
CaHCl	Ca $2p_{3/2}$	351.95	2.88	3.67
	Ca $2p_{1/2}$	355.62	2.34	
	Cl $2p_{3/2}$	202.75	2.25	1.57
	Cl $2p_{1/2}$	204.32	2.01	
$CaBr_2$	Ca $2p_{3/2}$	348.24	1.79	3.51
	Ca $2p_{1/2}$	351.75	1.83	
	Br $3p_{3/2}$	182.86	2.62	6.68
	Br $3p_{1/2}$	189.54	2.36	
CaHBr	Ca $2p_{3/2}$	347.36	2.38	3.59
	Ca $2p_{1/2}$	350.95	2.02	
	Ca $2p_{3/2}$	349.06	1.85	3.41
	Ca $2p_{1/2}$	352.47	1.60	
	Br $3p_{3/2}$	182.86	3.16	6.66
	Br $3p_{1/2}$	189.52	2.97	
CaI_2	Ca $2p_{3/2}$	356.08	2.15	2.54
	Ca $2p_{1/2}$	358.62	2.11	
	I $3d_{5/2}$	624.27	2.38	11.51
	I $3d_{3/2}$	635.78	2.33	
CaHI	Ca $2p_{3/2}$	352.05	3.08	3.86
	Ca $2p_{1/2}$	355.91	2.63	
	I $3d_{5/2}$	624.0[illegible]	2.57	11.54
	I $3d_{3/2}$	635.[illegible]7	2.46	

[a]Uncalibrated, except for $CaBr_2$ and CaHBr.

to $KHCO_3$ formed from air exposure of K during sample handling. The additional sharp peak at 4.3 ppm shown in Fig. 25b is assigned to water in the KCl crystals. The additional broad peak at 4.6 ppm shown in Fig. 25c is assigned KOH formed from air exposure of KH during sample handling.

The presence of KCl does not shift the resonance of ordinary hydride. The resonance at 1.1 ppm which is assigned to ordinary hydride ion was observed in the spectrum of the KHCl sample as shown in Fig. 25a. The distinct 0.8 and 1.1 ppm resonances could not be resolved if they were present. A large distinct upfield resonance was observed at −4.6 ppm which was not observed in either control. This upfield shifted peak is consistent with a hydride ion with a smaller radius as compared with ordinary hydride since a smaller radius increases the shielding or diamagnetism. The −4.6 ppm peak is assigned to a novel hydride ion that has a smaller radius than that of ordinary hydride ion since the shift was extraordinarily far upfield in the case of the KHCl sample. An additional water peak was found is other samples in which the novel hydride peak was observed. The presence of a water peak may demonstrate that the novel

Table 3
The results of the determination of the binding energies of selected core level electrons, full width at half maximum of the peaks, and energy of spin-orbit splitting for strontium halido hydrides compared with the corresponding strontium halides

Compound	Peak	Binding energy (eV)[a]	Full width at half maximum (FWHM) (eV)	Energy of spin-orbit splitting (eV)
SrF_2	Sr $3d_{5/2}$	140.46	2.13	1.81
	Sr $3d_{3/2}$	142.27	1.77	
	F 1s	691.12	2.11	
SrHF	Sr $3d_{5/2}$	139.20	2.48	1.91
	Sr $3d_{3/2}$	141.11	1.95	
	F 1s	689.88	2.42	
$SrCl_2$	Sr $3d_{5/2}$	139.45	2.36	1.86
	Sr $3d_{3/2}$	141.31	1.88	
	Cl $2p_{3/2}$	203.61	2.06	1.70
	Cl $2p_{1/2}$	205.31	1.95	
SrHCl	Sr $3d_{5/2}$	138.71	2.61	1.81
	Sr $3d_{3/2}$	140.52	1.99	
	Cl $2p_{3/2}$	202.98	2.06	1.72
	Cl $2p_{1/2}$	204.70	1.89	
$SrBr_2$	Sr $3d_{5/2}$	139.52	1.58	1.7
	Sr $3d_{3/2}$	141.22	1.65	
	Br $3p_{3/2}$	187.45	2.50	6.77
	Br $3p_{1/2}$	194.22	2.17	
SrHBr	Sr $3d_{5/2}$	138.56	1.33	1.96
	Sr $3d_{3/2}$	140.52	1.62	
	Sr $3d_{5/2}$	136.69	1.95	2.60
	Sr $3d_{3/2}$	139.29	1.55	
	Br $3p_{3/2}$	186.56	2.77	6.68
	Br $3p_{1/2}$	193.24	2.43	

[a]Uncalibrated, except for $SrBr_2$ and SrHBr.

hydride is stable to water, in the case that the water is not associated with unreacted KCl alone. This could partially explain why the KHCl sample was observed to be insoluble in water.

3.3.3. NMR of potassium bromo hydride sample

The ^1H MAS NMR spectra of the KHBr sample, the control comprising an equal molar mixture of KH and KBr, and the control KH relative to external tetramethylsilane (TMS) are shown in Figs. 26a, b, and c, respectively. Ordinary hydride ion has a resonance at 1.1 and 0.8 ppm in the KH/KBr mixture and in KH alone as shown in Figs. 26b and 26c, respectively. The additional sharp peaks at 4.3 and 5.9 ppm shown in Fig. 26a are assigned to water and $KHCO_3$ formed from air exposure of K during sample handling. The additional sharp peak at 4.2 ppm shown in Fig. 26b is assigned to water in the KBr crystals. The additional broad peak at 4.6 ppm shown in Fig. 26c is assigned KOH formed from air exposure of KH during sample handling.

The presence of KBr does not shift the resonance of ordinary hydride. The resonance at 1.2 ppm which is assigned to ordinary hydride ion was observed in the spectrum of the KHBr sample as shown in Fig. 26a. The distinct 0.8 and 1.1 ppm resonances could not be resolved if they were present. A large distinct upfield resonance was observed at −4.1 ppm which was not observed in either control. This upfield shifted peak is consistent with a hydride ion with a smaller radius as compared with ordinary hydride since a

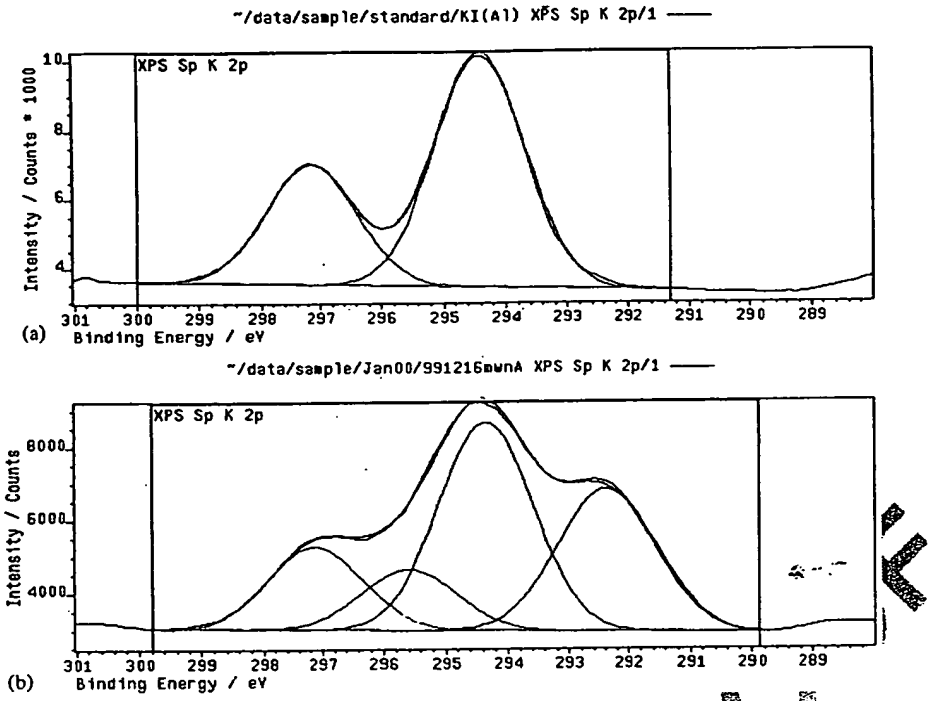

Fig. 19. (a) The XPS spectra of the K 2p core level in KI. (b) The XPS spectra of the K 2p core level in KHI.

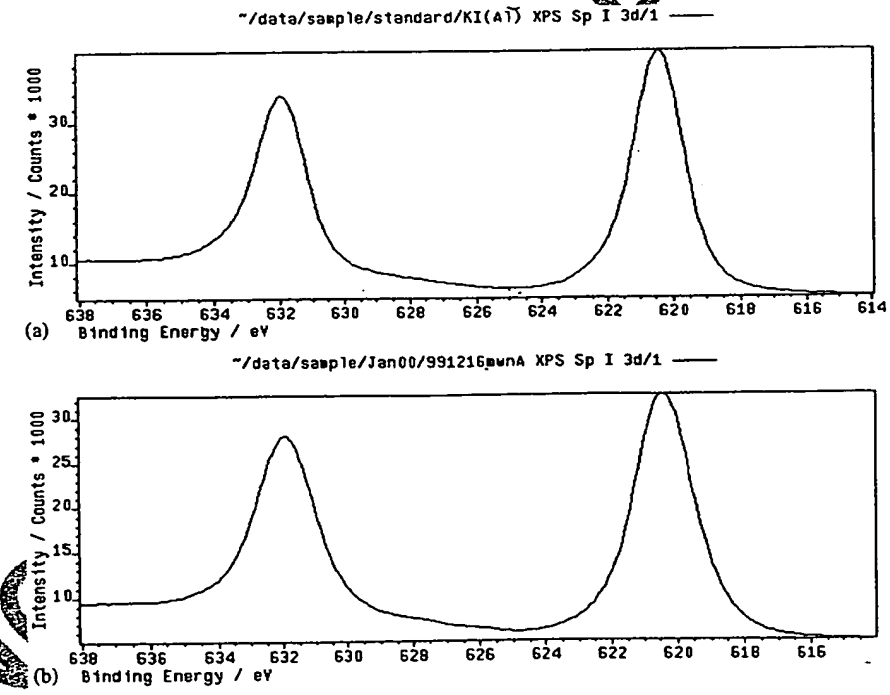

Fig. 20. (a) The XPS spectra of the I 3d core level in KI. (b) The XPS spectra of the I 3d core level in KHI.

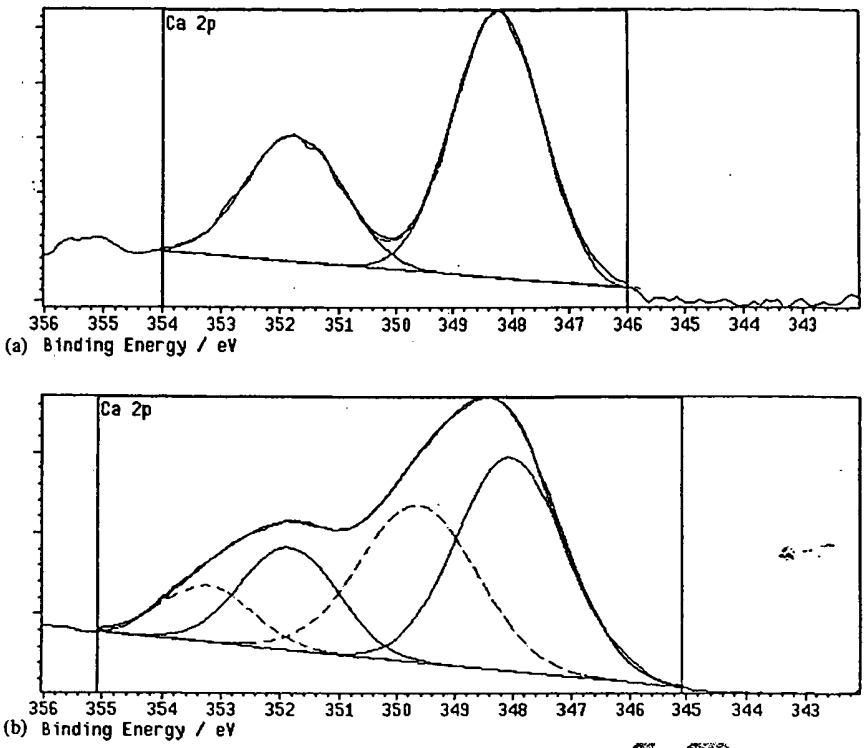

Fig. 21. (a) The XPS spectra of the Ca 2p core level in $CaBr_2$. (b) The XPS spectra of the Ca 2p core level in CaHBr.

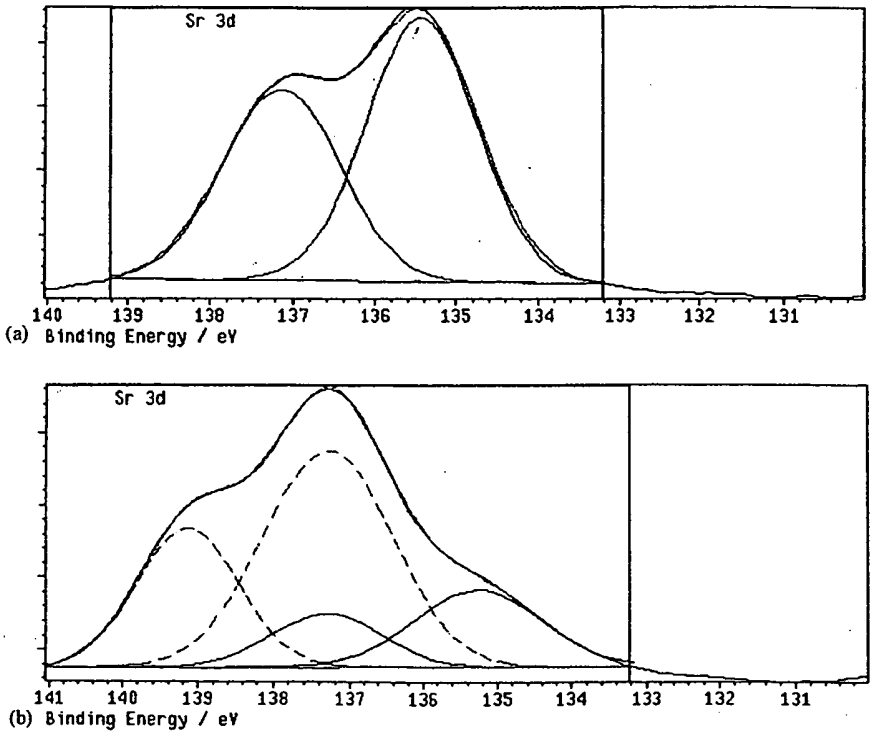

Fig. 22. (a) The XPS spectra of the Sr 3d core level in $SrBr_2$. (b) The XPS spectra of the Sr 3d core level in SrHBr.

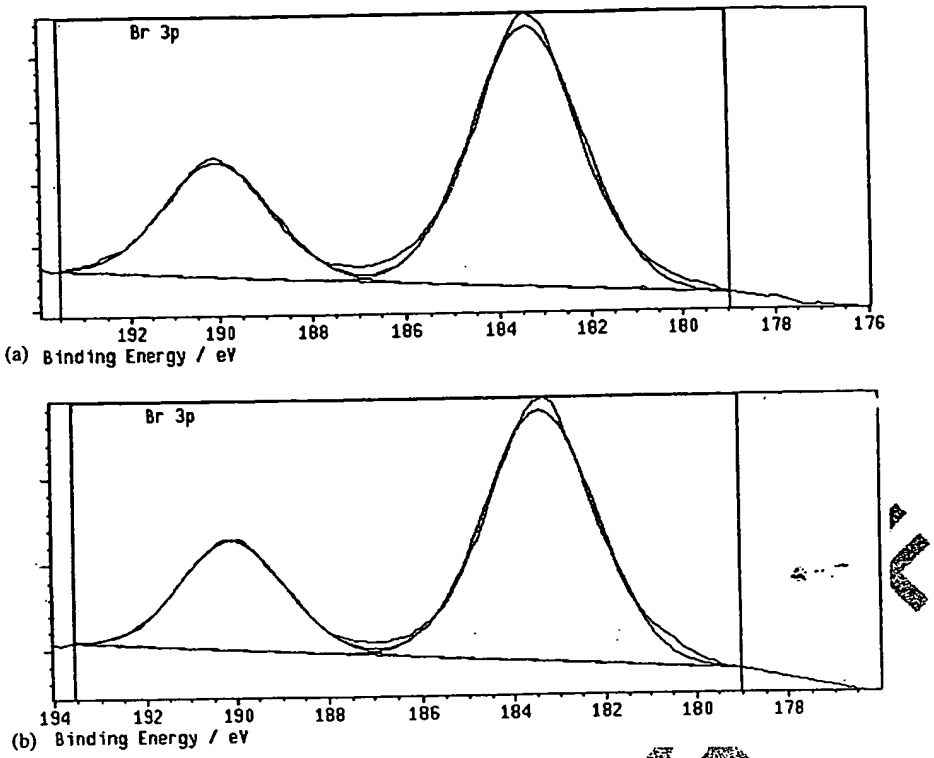

Fig. 23. (a) The XPS spectra of the Br 2p core level in $SrBr_2$. (b) The XPS spectra of the Br 2p core level in SrHBr.

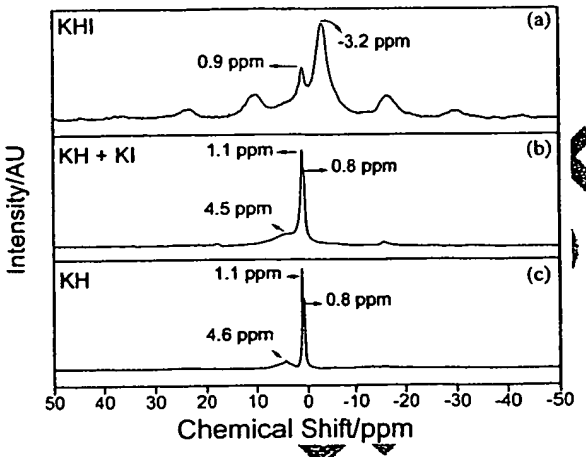

Fig. 24. (a) The ^1H MAS NMR spectrum of KHI relative to external tetramethylsilane (TMS). (b) The ^1H MAS NMR spectrum of the control comprising an equal molar mixture of KH and KI relative to external tetramethylsilane (TMS). (c) The ^1H MAS NMR spectrum of the control KH relative to external tetramethylsilane (TMS).

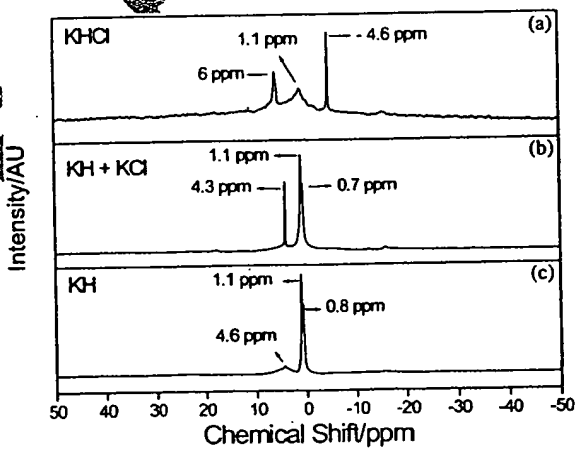

Fig. 25. (a) The ^1H MAS NMR spectrum of KHCl relative to external tetramethylsilane (TMS). (b) The ^1H MAS NMR spectrum of the control comprising an equal molar mixture of KH and KCl relative to external tetramethylsilane (TMS). (c) The ^1H MAS NMR spectrum of the control KH relative to external tetramethylsilane (TMS).

smaller radius increases the shielding or diamagnetism. The −4.1 ppm peak is assigned to a novel hydride ion that has a smaller radius than that of ordinary hydride ion since the shift was extraordinarily far upfield in the case of the KHBr sample.

3.3.4. *NMR of rubidium fluoro hydride sample*

The ^1H MAS NMR spectrum of RbHF relative to external tetramethylsilane (TMS) is shown in Fig. 27a. Distinguishable resonances were observed at 1.2 and −4.4 ppm. The

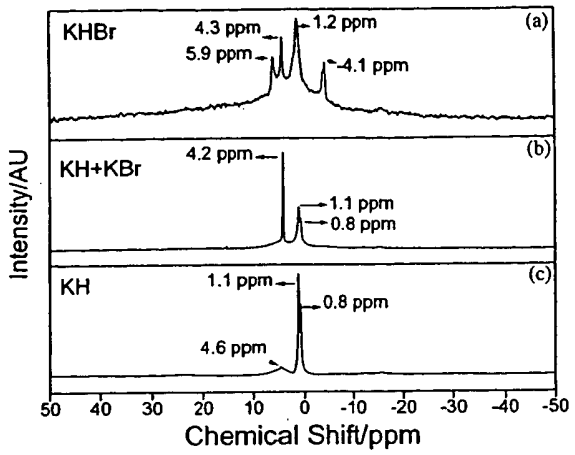

Fig. 26. (a) The ^{1}H MAS NMR spectrum of KHBr relative to external tetramethylsilane (TMS). (b) The ^{1}H MAS NMR spectrum of the control comprising an equal molar mixture of KH and KBr relative to external tetramethylsilane (TMS). (c) The ^{1}H MAS NMR spectrum of the control KH relative to external tetramethylsilane (TMS).

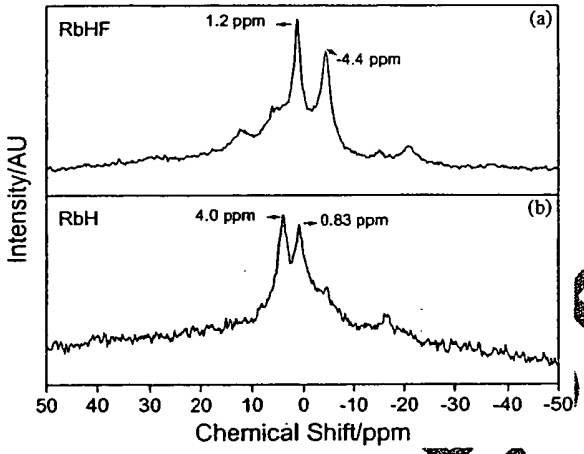

Fig. 27. (a) The ^{1}H MAS NMR spectrum of RbHF relative to external tetramethylsilane (TMS). (b) The ^{1}H MAS NMR spectrum of the control RbH relative to external tetramethylsilane (TMS).

upfield peak is assigned to a novel hydride ion of RbHF. The down field shifted peak may be ordinary hydride in a different chemical environment. The ^{1}H MAS NMR spectrum of the control RbH relative to external tetramethylsilane (TMS) is shown in Fig. 27b. The 0.83 ppm peak is assigned to ordinary hydride ion of RbH. The peak at 4.0 ppm is assigned to RbOH formed from air exposure of RbH during sample handling.

The upfield shifted peak observed in the RbHF sample is consistent with a hydride ion with a smaller radius as compared with ordinary hydride since a smaller radius increases the shielding or diamagnetism. The −4.4 ppm peak is assigned to a novel hydride ion that has a smaller radius than that of ordinary hydride ion since the shift was extraordinarily far upfield in the case of the RbHF sample.

3.3.5. NMR of strontium bromo hydride sample

The SrHBr sample was not spun; so, the hydride peaks were not resolved. Instead valuable ^{1}H–^{1}H separation data as well as ^{1}H content was obtained. The ^{1}H MAS NMR spectra of SrHBr relative to external H_2O is shown in Fig. 28. The sample contained a significant amount of hydrogen with an integration of 0.0983 mmoles corresponding to about 0.02 wt% ^{1}H in the sample. There are two components: a narrow component with a peak at 6.3 ppm having an area of approximately 1/4th of the total signal, and a broad signal with a width of about 60 kHz. The broadening of the peak corresponds to ^{1}H–^{1}H separation of under 1.5 Å. This is very significant given that the unit cell (orthorhombic P_{nma} form) parameters for ordinary strontium hydride are $a = 7.358$ Å, $b = 6.377$ Å and $c = 3.882$ Å. The seven short M–H distances are 2.49 Å. The two long M–H distances are 3.06 Å. The H$^-$ radius is 1.39 Å [11]. The data is consistent with a novel hydride ion of a greatly reduced radius.

3.4. Gas chromatography (GC)

The gas chromatograph of the normal hydrogen gave the retention time for para hydrogen and ortho hydrogen as 14.5 and 16.5 min, respectively. Control $SrBr_2$ showed no hydrogen release upon heating to above 600°C. The gas chromatograph of the dihydrino (see Appendix) or hydrogen released from the SrHBr sample when it was heated to above 600°C is shown in Fig. 29. This chromatograph is representative of the results of the determination of dihydrino or hydrogen released from each sample of MHX or MHMX when heated to 600°C. In the case of a very stable hydride, no hydrogen may be released, thus, the amount observed in the minimum content. Table 4 gives a results which are representative of the minimum dihydrino or hydrogen content of novel hydride compounds determined by gas chromatograph of the gas released from each sample when it was heated to above 600°C. Each control, MX or MX_2, showed no hydrogen release upon heating to above 600°C.

3.5. Mass spectroscopy (MS)

The dihydrino (see Appendix) was identified in the gas released by thermal decomposition of solid samples by mass spectroscopy. Dihydrino was detected as a species with a mass to charge ratio of two ($m/e = 2$) that has a higher ionization potential than that of normal hydrogen by recording the ion current as a function of the electron gun energy. The intensity as a function of time for masses $m/e = 1$, $m/e = 2$,

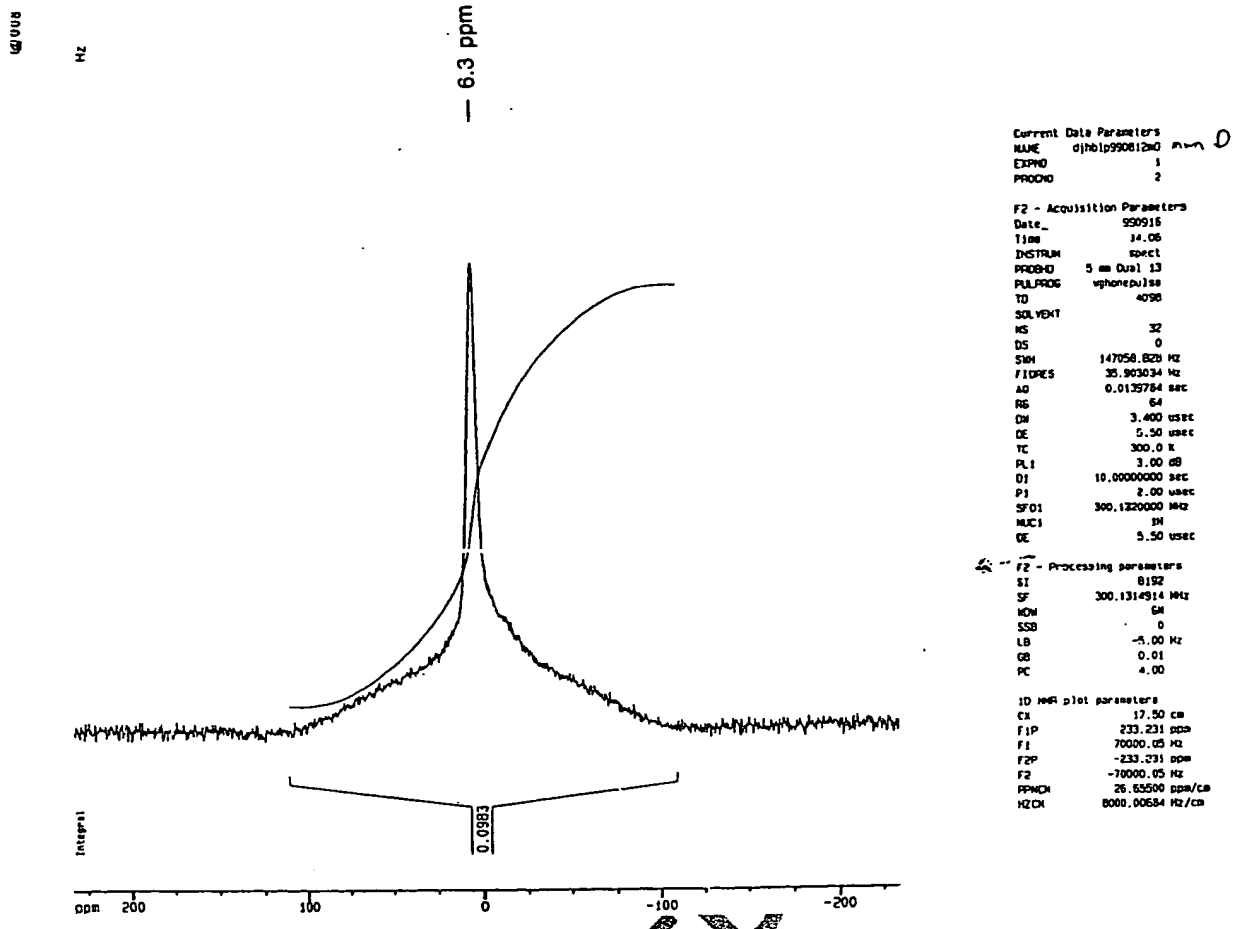

Fig. 28. The ^1H MAS NMR spectra of SrHBr relative to external H_2O.

and $m/e = 3$ obtained while changing the ionization potential (IP) of the mass spectrometer from 30 to 70 eV for ultrapure hydrogen is shown in Fig. 30. Upon increasing the ionization potential from 30 to 70 eV, typically the $m/e = 2$ ion current for the ultrapure hydrogen increased by a factor of less than 2.

The intensity as a function of time for masses $m/e = 1$, $m/e = 2$, and $m/e = 3$ obtained while changing the ionization potential (IP) of the mass spectrometer from 30 to 70 eV for gas released from thermal decomposition of the KHI sample is shown in Fig. 31. Upon increasing the ionization potential from 30 to 70 eV, typically the $m/e = 2$ ion current for the KHI sample increased by a factor of about 1000 under the same pressure conditions as those of the ultrapure hydrogen control. Fig. 31 is representative of the results of the determination of the increase in the $m/e = 2$ ion current for each sample of MHX or MHMX upon increasing the ionization potential from 30 to 70 eV under the same pressure conditions as those of the ultrapure hydrogen control.

The $m/e = 2$ ion current for the KHCl, KH $KHCO_3$, CsHI, SrHF, and SrHBr sample increased by a factor of about 400, 200, 400, 20, and 50, respectively, under the same pressure conditions as those of the ultrapure hydrogen control.

4. Conclusions

The ToF-SIMS, XPS, NMR, and thermal decomposition with analysis by GC, and MS results confirm the identification of novel hydride compounds MHX and MHMX wherein M is the metal, X, is a singly negatively charged anion, and H comprises a novel high binding energy hydride ion. The negative ToF-SIMS spectra of KHI, KH $KHCO_3$, RbHF, and SrHF were dominated by the hydride ion peak which identified the structures. The thermal decomposition with mass spectroscopic analysis indicated the minimum hydrogen or dihydrino content. At least $H^-(1/2)$ was observed to be present in KHX and KH $KHCO_3$.

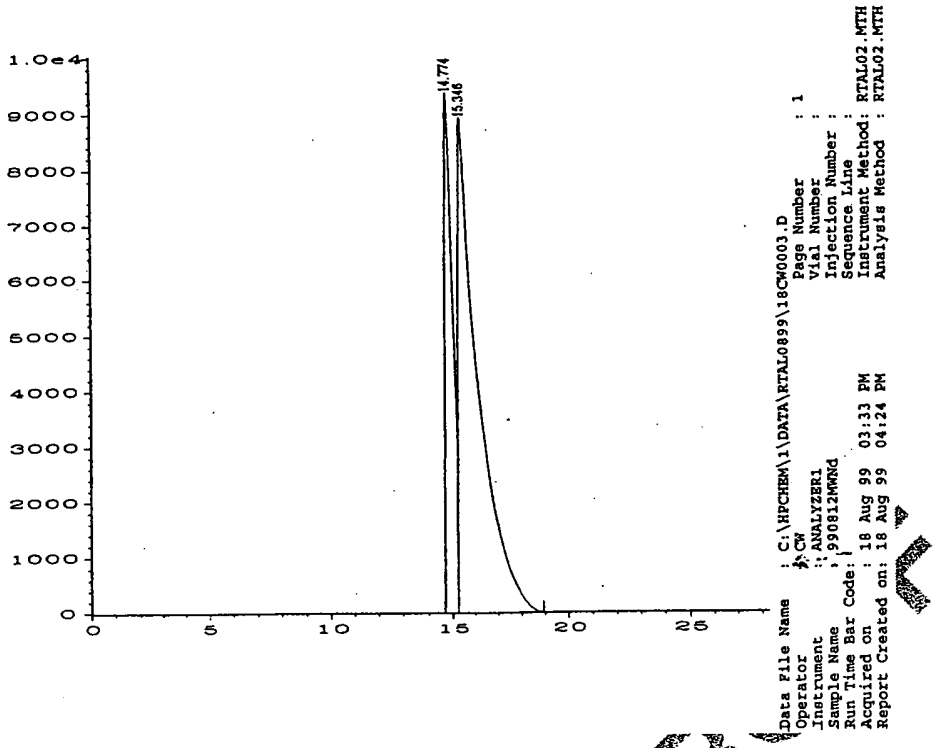

Fig. 29. The gas chromatograph of the dihydrino or hydrogen released from the SrHBr sample when it was heated to above 600°C.

Table 4
The minimum dihydrino or hydrogen content of novel hydride compounds determined by gas chromatograph of the gas released from each sample when it was heated to above 600°C

Novel hydride compound	Hydrogen or dihydrino content (μmol/g)
KHI	400
KHCl	200
$KHKHCO_3$	40
SrHF	100
SrHBr	1300

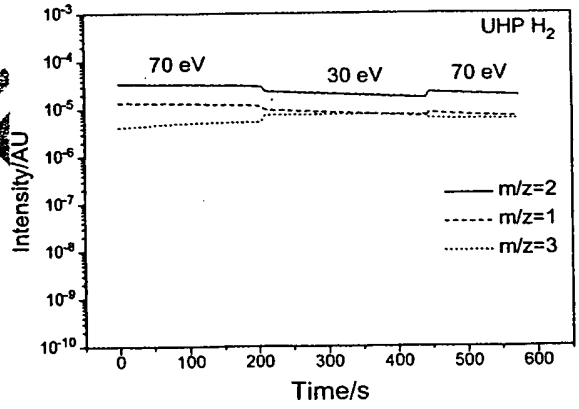

Fig. 30. The intensity as a function of time for masses $m/e = 1$, $m/e = 2$, and $m/e = 3$ obtained while changing the ionization potential (IP) of the mass spectrometer from 30 to 70 eV for ultrapure hydrogen.

The XPS of the low binding energy region of KHI is consistent with the presence of H^- ($n = 1/6$) $E_b = 22.8$ eV. This product is predicted by an autocatalysis reaction of two H(1/4) atoms formed via a potassium catalyst which has been confirmed by extreme ultraviolet spectroscopy [3]. The XPS of KHCl is consistent with the presence of a new peak at 36.7 eV which is in agreement with the predicted binding energy of $H^-(n = 1/8)$ $E_b = 36.1$ eV. The bonding of hydrino hydride ions with alkali and alkaline earth metals significantly broadens the metal core level peaks. The magnitude of broadening ranges from 0.3 to 0.9 eV, depending on compound. The trend for the broadening effect follows the sequence: iodo hydrides~bromo hydrides > fluoro hydrides~chloro hydrides. In particular, two additional spin-orbit splittings had to be added to each of potassium iodo hydride, calcium bromo hydride, and strontium bromo hydride in order to obtain a good curve fit of the K 2p, Ca 2p, and Sr 3d spectra, respectively.

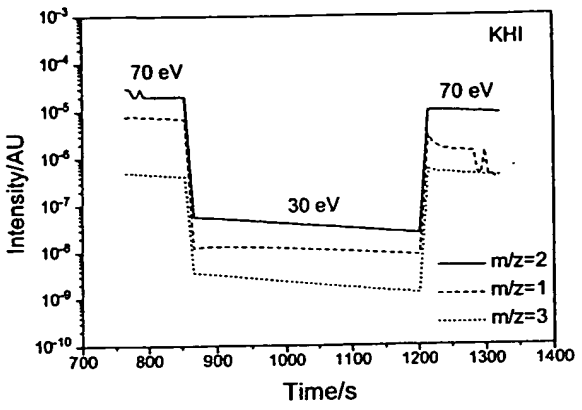

Fig. 31. The intensity as a function of time for masses $m/e = 1, m/e = 2$, and $m/e = 3$ obtained while changing the ionization potential (IP) of the mass spectrometer from 30 to 70 eV for gas released from thermal decomposition of the KHI sample.

Large distinct upfield resonances were observed at −3.2 ppm, −4.6 ppm, −4.1 ppm, −4.4 ppm in the case of KHI, KHCl, KHBr, and RbHF, respectively. The peaks are assigned to novel hydride ions that have substantially smaller radii than that of ordinary hydride ion since the shift was extraordinarily far upfield. The NMR peak of KHI at −3.2 ppm may be due to $H^-(n = 1/6)$ $E_b = 22.8$ eV observed by XPS. The NMR peak of KHCl at −4.6 ppm may be due to $H^-(n = 1/8)$ $E_b = 36.1$ eV observed by XPS. The NMR of SrHBr showed a ^1H–^1H separation of under 1.5 Å . This is very significant compared to the atomic spacing parameters of ordinary strontium hydride and is consistent with a novel hydride ion of a greatly reduced radius.

The chemical structure and properties of the present novel compounds are indicative of a new field of hydrogen chemistry. Novel hydride ions may combine with other cations such as other alkali cations and alkaline earth, rare earth, and transition element cations. Numerous novel compounds may be synthesized with extraordinary properties relative to the corresponding compounds having ordinary hydride ions. These novel compounds may have a breath of applications. For example, a high voltage battery according to the hydride binding energies observed by XPS may be possible having projected specifications that surpass those of the internal combustion engine. The discovery of a novel hydride ion with a high binding energy has implications for a new field of hydride chemistry with applications such as a high voltage battery [9].

Hydride ions having extraordinary binding energies may stabilize a cation M^{x+} in an extraordinarily high oxidation state such as +2 in the case of lithium. Thus, these hydride ions may be used as the basis of a high voltage battery of a rocking chair design wherein the hydride ion moves back and forth between the cathode and anode half cells during discharge and charge cycles. Exemplary reactions for a cation M^{x+} are:

Cathode reaction:

$$MH_x + e^- \rightarrow MH_{x-1} + H^- \quad (1)$$

Anode reaction:

$$MH_{x-2} + H^- \rightarrow MH_{x-1} + e^- \quad (2)$$

Overall reaction:

$$MH_x + MH_{x-2} \rightarrow 2MH_{x-1}. \quad (3)$$

Appendix A.

It has been reported that intense extreme ultraviolet (EUV) emission was observed at low temperatures (e.g. $\approx 10^3$ K) from atomic hydrogen and certain atomized elements or certain gaseous ions which ionize at integer multiples of the potential energy of atomic hydrogen, 27.2 eV [1–6]. The mechanism of EUV emission can not be explained by the conventional chemistry of hydrogen, but it is predicted by a solution of the Schrodinger equation with a nonradiative boundary constraint put forward by Mills [12,13]. The energy release must result in a lower-energy state of hydrogen. Mills predicts that certain atoms or ions serve as catalysts to release energy from hydrogen to produce an increased binding energy hydrogen atom called a *hydrino atom* having a binding energy of

$$\text{Binding Energy} = \frac{13.6 \text{ eV}}{n^2} \quad (A.1)$$

where

$$n = \frac{1}{2}, \frac{1}{3}, \frac{1}{4}, \ldots, \frac{1}{p} \quad (A.2)$$

and p is an integer greater than 1, designated as $H[a_H/p]$ where a_H is the radius of the hydrogen atom. Hydrinos are predicted to form by reacting an ordinary hydrogen atom with a catalyst having a net enthalpy of reaction of about

$$m \cdot 27.2 \text{ eV} \quad (A.3)$$

where m is an integer. This catalysis releases energy from the hydrogen atom with a commensurate decrease in size of the hydrogen atom, $r_n = na_H$. For example, the catalysis of $H(n = 1)$ to $H(n = 1/2)$ releases 40.8 eV, and the hydrogen radius decreases from a_H to $\frac{1}{2}a_H$.

The excited energy states of atomic hydrogen are also given by Eq. (A.1) except that

$$n = 1, 2, 3, \ldots \quad (A.4)$$

The $n = 1$ state is the "ground" state for "pure" photon transitions (the $n = 1$ state can absorb a photon and go to an excited electronic state, but it cannot release a photon and go to a lower-energy electronic state). However, an electron transition from the ground state to a lower-energy state is possible by a nonradiative energy transfer such as multipole coupling or a resonant collision mechanism. These

lower-energy states have fractional quantum numbers, $n = 1/\text{integer}$. Processes that occur without photons and that require collisions are common. For example, the exothermic chemical reaction of H + H to form H_2 does not occur with the emission of a photon. Rather, the reaction requires a collision with a third body, M, to remove the bond energy $-H + H + M \rightarrow H_2 + M^*$ [14]. The third body distributes the energy from the exothermic reaction, and the end result is the H_2 molecule and an increase in the temperature of the system. Some commercial phosphors are based on nonradiative energy transfer involving multipole coupling. For example, the strong absorption strength of Sb^{3+} ions along with the efficient nonradiative transfer of excitation from Sb^{3+} to Mn^{2+}, are responsible for the strong manganese luminescence from phosphors containing these ions [15]. Similarly, the $n = 1$ state of hydrogen and the $n = 1/\text{integer}$ states of hydrogen are nonradiative, but a transition between two nonradiative states is possible via a nonradiative energy transfer, say $n = 1$ to $n = 1/2$. In these cases, during the transition the electron couples to another electron transition, electron transfer reaction, or inelastic scattering reaction which can absorb the exact amount of energy that must be removed from the hydrogen atom. Thus, a catalyst provides a net positive enthalpy of reaction of $m \cdot 27.2$ eV (i.e. it absorbs $m \cdot 27.2$ eV where m is an integer). Certain atoms or ions serve as catalysts which resonantly accept energy from hydrogen atoms and release the energy to the surroundings to effect electronic transitions to fractional quantum energy levels.

A.1. Inorganic catalysts

A catalytic system is provided by the ionization of t electrons from an atom to a continuum energy level such that the sum of the ionization energies of the t electrons is approximately $m \cdot 27.2$ eV where m is an integer. One such catalytic system involves strontium. The first through the fifth ionization energies of strontium are 5.69484, 11.0301, 42.89, 57, and 71.6 eV, respectively [16]. The ionization reaction of Sr to Sr^{5+} ($t = 5$), then, has a net enthalpy of reaction of 188.2 eV, which is equivalent to $m = 7$ in Eq. (A.3).

$$188.2 \text{ eV} + \text{Sr}(m) + \text{H}\left[\frac{a_H}{p}\right] \rightarrow \text{Sr}^{5+} + 5e^- + \text{H}\left[\frac{a_H}{(p+7)}\right] + [(p+7)^2 - p^2]X13.6 \text{ eV}, \quad (A.5)$$

$$\text{Sr}^{5+} + 5e^- \rightarrow \text{Sr}(m) + 188.2 \text{ eV} \quad (A.6)$$

And, the overall reaction is

$$\text{H}\left[\frac{a_H}{p}\right] \rightarrow \text{H}\left[\frac{a_H}{(p+7)}\right] + [(p+7)^2 - p^2]X13.6 \text{ eV}. \quad (A.7)$$

Another catalytic system that is provided by the ionization of t electrons from an atom to a continuum energy level such that the sum of the ionization energies of the t electrons is approximately $mX27.2$ eV where m is an integer involves potassium. The first, second, and third ionization energies of potassium are 4.34066, 31.63, 45.806 eV, respectively [16]. The triple ionization ($t = 3$) reaction of K to, K^{3+} then, has a net enthalpy of reaction of 81.7426 eV, which is equivalent to $m = 3$ in Eq. (A.3).

$$81.7426 \text{ eV} + \text{K}(m) + \text{H}\left[\frac{a_H}{p}\right] \rightarrow \text{K}^{3+} + 3e^- + \text{H}\left[\frac{a_H}{(p+3)}\right] + [(p+3)^2 - p^2]X13.6 \text{ eV}, \quad (A.8)$$

$$\text{K}^{3+} + 3e^- \rightarrow \text{K}(m) + 81.7426 \text{ eV}. \quad (A.9)$$

And, the overall reaction is

$$\text{H}\left[\frac{a_H}{p}\right] \rightarrow \text{H}\left[\frac{a_H}{(p+3)}\right] + [(p+3)^2 - p^2]X13.6 \text{ eV}. \quad (A.10)$$

A novel hydride ion having extraordinary chemical properties given by Mills [12] is predicted to form by the reaction of an electron with a hydrino (Eq. (A.11)). The resulting hydride ion is referred to as a hydrino hydride ion, designated as $H^-(1/p)$.

$$\text{H}\left[\frac{a_H}{p}\right] + e^- \rightarrow \text{H}^-(1/p) \quad (A.11)$$

The hydrino hydride ion is distinguished from an ordinary hydride ion having a binding energy of 0.8 eV. The hydrino hydride ion is predicted [12] to comprise a hydrogen nucleus and two indistinguishable electrons at a binding energy according to the following formula:

$$\text{Binding Energy} = \frac{\hbar^2\sqrt{s(s+1)}}{8\mu_e a_0^2\left[\frac{1+\sqrt{s(s+1)}}{p}\right]^2} - \frac{\pi\mu_0 e^2\hbar^2}{m_e^2 a_0^3}\left(1 + \frac{2^2}{\left[\frac{1+\sqrt{s(s+1)}}{p}\right]^3}\right) \quad (A.12)$$

where p is an integer greater than one, $s = 1/2$, π is pi, $\hbar$ is Planck's constant bar, μ_0 is the permeability of vacuum, m_e is the mass of the electron, μ_e is the reduced electron mass, a_0 is the Bohr radius, and e is the elementary charge. The ionic radius is

$$r_1 = \frac{a_0}{p}(1 + \sqrt{s(s+1)}); \quad s = \frac{1}{2} \quad (A.13)$$

From Eq. (A.13), the radius of the hydrino hydride ion $H^-(1/p)$; p = integer is $1/p$ that of ordinary hydride ion, $H^-(1/1)$. Compounds containing hydrino hydride ions have been isolated as products of the reaction of atomic hydrogen with atoms and ions identified as catalysts by EUV emission [1–6,17–20].

Alkali and alkaline earth hydrides react violently with water to release hydrogen gas which subsequently ignites due to the exothermic reaction with water. Typically metal

hydrides decompose upon heating at a temperature well below the melting point of the parent metal. These saline hydrides, so called because of their saltlike or ionic character, are the monohydrides of the alkali metals and the dihydrides of the alkaline-earth metals. Mills predicts a hydrogen-type molecule having a first binding energy of about

$$\text{Binding Energy} = \frac{15.5}{(\frac{1}{p})^2}\text{eV}. \qquad \text{(A.14)}$$

Dihydrino molecules may be produced by the thermal decomposition of hydrino hydride ions. $KH^-(1/2)$ may be less reactive and more thermally stable than ordinary potassium hydride, but may react at high temperature to form a hydrogen-type molecule. For example, potassium iodo hydride KH(1/2)I may be heated to release dihydrino by thermal decomposition.

$$2KH(1/2)I \xrightarrow{\Delta} H_2^* \left[2c' = \frac{a_0}{\sqrt{2}}\right] + 2KI \qquad \text{(A.15)}$$

where $2c'$ is the internuclear distance and a_0 is the Bohr radius [12]. The possibility of releasing dihydrino by thermally decomposing alkali and alkaline earth halido hydrides and KH $KHCO_3$ with identification by gas chromatography was explored.

The first ionization energy, IP_1, of the dihydrino molecule

$$H_2^* \left[2c' = \frac{\sqrt{2}a_0}{2}\right] \rightarrow H_2^*[2c' = a_0]^+ + e^- \qquad \text{(A.16)}$$

is $IP_1 = 62$ eV ($p=2$ in Eq. (A.14)); whereas, the first ionization energy of ordinary molecular hydrogen, $H_2[2c' = \sqrt{2}a_0]$, is 15.46 eV. Thus, the possibility of using mass spectroscopy to discriminate $H_2[2c' = \sqrt{2}a_0]$ from $H_2^*[2c' = a_0/\sqrt{2}]$ on the basis of the large difference between the ionization energies of the two species was explored. A novel high binding energy hydrogen molecule assigned to dihydrino $H_2^*[2c' = a_0/\sqrt{2}]$ was identified by the thermal decomposition of alkali and alkaline earth halido hydrides and KH $KHCO_3$ with analysis by gas chromatography, and mass spectroscopy.

References

[1] Mills R, Dong J, Lu, Y. Observation of extreme ultraviolet hydrogen emission from incandescently heated hydrogen gas with certain catalysts. Pacific Conference on Chemistry and Spectroscopy and the 35th ACS Western Regional Meeting, Ontario Convention Center, California, October 6–8, 1999.

[2] Mills R, Dong J, Lu Y. Observation of extreme ultraviolet hydrogen emission from incandescently heated hydrogen gas with certain catalysts. Int J Hydrogen Energy 2000;25:919–43.

[3] Mills R. Observation of extreme ultraviolet emission from hydrogen-KI plasmas produced by a hollow cathode discharge. Int J Hydrogen Energy, submitted for publication.

[4] Mills R. Temporal behavior of light-emission in the visible spectral range from a Ti-K2CO3-H-Cell. Int J Hydrogen Energy, accepted.

[5] Mills R, Lu R, Onuma T. Formation of a hydrogen plasma from an incandescently heated hydrogen-potassium gas mixture and plasma decay upon removal of heater power. Int J Hydrogen Energy, accepted.

[6] Mills R, Nansteel M, Lu Y. Observation of extreme ultraviolet hydrogen emission from incandescently heated hydrogen gas with strontium that produced an optically measured power balance that was 4000 times the control. Int J Hydrogen Energy, accepted.

[7] Microsc. Microanal. Microstruct., 3(1) 1992.

[8] PHI Trift II, ToF-SIMS Technical Brochure, Eden Prairie, MN 55344, USA, 1999.

[9] Mills R. Novel inorganic hydride. Int J Hydrogen Energy 2000;25:669–83.

[10] Briggs D, Seah MP, editors. Practical surface analysis, 2nd ed. Ion and neutral spectroscopy, vol. 2. New York: Wiley, 1992.

[11] Mackay K.M. Hydrogen Compounds of the metallic elements. London: E. & F. N. Spon, 1966.

[12] Mills R. The grand unified theory of classical quantum Mechanics. Cranbury, NJ: BlackLight Power, Inc. January 2000. Distributed by Amazon.com.

[13] Mills R. The hydrogen atom revisited. Int J Hydrogen Energy, accepted.

[14] Sidgwick NV. The chemical elements and their compounds, vol. I. Oxford: Clarendon Press, 1950. p. 17.

[15] Lamb MD. Luminescence spectroscopy. London: Academic Press, 1978. p. 68.

[16] Linde DR. CRC handbook of chemistry and physics, 79th ed. Boca Raton, FL: CRC Press, (1998–9). pp. 10-175–10-177.

[17] Mills R, Dhandapani B, Greenig N, He J. Synthesis and characterization of potassium iodo hydride. Int J Hydrogen Energy, accepted.

[18] Mills R. Novel hydrogen compounds from a potassium carbonate electrolytic cell. Fusion Technol 2000;37(2):157–82.

[19] Mills R, He J, Dhandapani B. Novel hydrogen compounds. 1999 Pacific Conference on Chemistry and Spectroscopy and the 35th ACS Western Regional Meeting, Ontario Convention Center, California, October 6–8, 1999.

[20] Mills R. Highly stable novel inorganic hydrides. J Mater Res, submitted for publication.